1-1-2016

Electrocatalysis In Li-S Batteries

Hesham I. Al Salem
Wayne State University,

ELECTROCATALYSIS IN LI-SULFUR BATTERIES

by

HESHAM I. A. AL SALEM

DISSERTATION

Submitted to the graduate school

of Wayne State University,

Detroit, Michigan

in partial fulfillment of requirements

for the degree of

DOCTOR OF PHILOSOPHY

2016

MAJOR: MECHANICAL ENGINEERING

Approved By:

_____

Advisor Date

_____

_____

_____

_____

DEDICATION

TO MY LOVELY WIFE DAAD, MY KIDS (The M FAMILY - MAHDI, MARWAN,

MOHAMMAD AND MOSTAFA) AND TO MY PARENTS

ACKNOWLEDGEMENTS

I would like to express my deepest gratitude and thanks Dr. Leela Mohana Reddy Arava as my true and real advisor for doctorate research in the past years. We were closely working together during this unforgettable time period in my life. I don't even remember how many nights we were fabricating cells and doing mixing, filtration and centrifugation until midnight. His kindness, patience, and dedication to battery research always make me very impressive. I literally appreciate his help, advice and discussion as a friend in my research work. Also, I would like to thank my advisory committee, Dr. Golam Newaz, Dr. Guru Dinda and Dr. Mahendra Kavdia for their helps and supports. Special thank also for Dr. Babu Ganguli for being my mentor and shock absorber and always encouraging me, sharing his research stories with me. Also thank Dr. Chitturi for his precious discussion and teachings. I am very grateful to Ehab Abdelhamid for his warmest talking magnificent helps. Thank Dr. Amessou for helping me to doing a lot of experiment in the chemistry department and for introducing me to a new friends and techniques. Great thanks for the lab king - Khalid Abbabtin for his best suggestions. He is a true brother and a supporter. Also special thanks for Abdulrazzag Sawas for the uncountable helps, supports and patience. Great thanks to Deepesh for his proofreading support and silent joys he used to bring to the lab.

I particularly have to thank my wife, Daad Al-mansour, with all my heart for her sacrifice and companionship during the past years. Her food was really amazing. Everyone in our group taste and enjoy her wonderful sweets. Not a word could express my truly gratitude and love to her. I would never complete my research work without her support and understanding.

Also thank my big 4 trouble makers (Mahdi, Marwan, Mohammad and Mostafa). They are really adorable kids. I was so happy we could still get together in my journey of graduate studies. Special thanks to my parents, parents in law, brothers and sisters who have been always supporting

me and giving me the courage to do what I wanted to do. I always thank them for teaching me how to be an educated person since I was little. This work would not have been possibly finished without their fully support and pray. I miss them all and I am seeking there happiness.

TABLE OF CONTENTS

LIST OF TABLES

LIST OF FIGURES

CHAPTER 1 INTRODUCTION

1.1 Lithium ion batteries and their significance

The ubiquitous growth in portability of both handheld electronics as well as electric vehicles has largely been fueled by the progress made in electrochemical energy storage. Current Li-ion battery has a rich history of innovations. It all started with the discovery of intercalation of Li-ions reversibly into graphite structure, known to be anode, wherein van der Walls forces drive the Li-ions between graphene sheets at a low potential close to the Li/Li^+. As a complementary to anode, another important invention happened in the form of lithium intercalation compounds primarily based on lithiated transition metal oxides such as $LiCoO_2$, $LiNO_2$ etc. as cathode materials. With these fundamental breakthroughs namely graphitic carbon as anode and $LiCoO_2$ as cathode, Sony corporation was first introduced commercial Li-ion battery in 1991[1]. Later on, a lot of advancement have been noticed for lithium ion batteries regarding the specific capacity, safety, cycle life, materials and configurations [2].

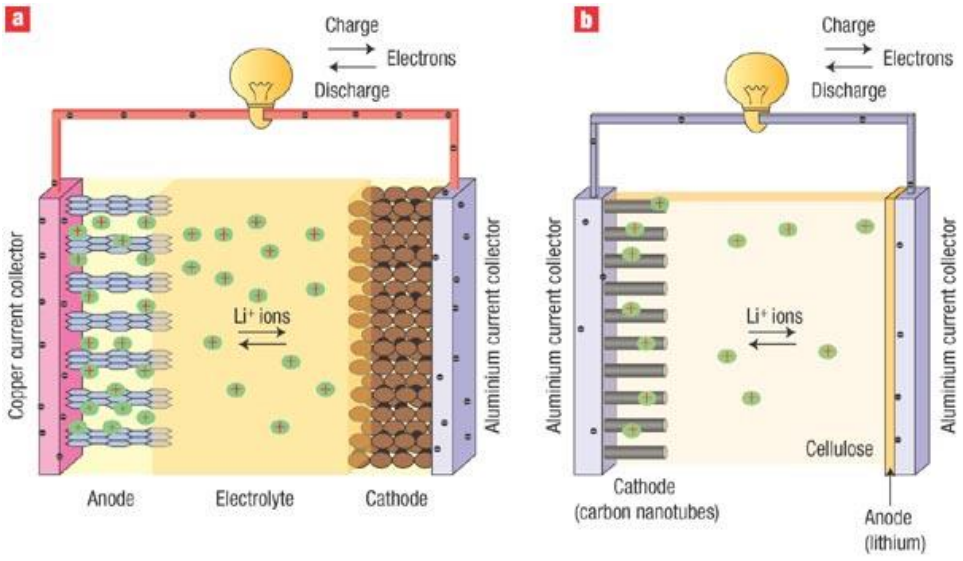

Figure 1-1 Working principle of Li-ion battery[3]

In principle, Lithium-ion battery uses a cathode (positive electrode), an anode (negative electrode) separated by a polymer separator and electrolyte as ionic conductor. During charge process, the Li-ions flow from the cathode to anode through the electrolyte and separator; discharge reverses the direction of the ions and at the same time, electrons are liberated at anode and travel to an outside electric circuit to do the work (Figure 1-1) [2, 4-6].

Lithium ion batteries have a wide range of applications due to its unique advantages over other rechargeable batteries, such as:

- High energy and power density compared to other rechargeable batteries (twice as much as Ni-Cd battery)[2]
- Higher cell voltage up to 4V per cell with longer charge retention or shelf life
- High cycle numbers with extended service hours, light weight and smaller size
- Wide temperature range of operation (-40 to + 70 ^{o}C)
- Very low rate of self-discharge with no memory effect
- High current-rate capability

1.2 Limitations of lithium ion batteries

The growth of population, economics and advancement in the modern e-society required energy storage devices with high energy density and extended cycle life. Despite all the aforementioned advantages of lithium ion batteries, the ability to meet the ever-increasing energy demands from both portable electronics and modern electric vehicles has posed serious concern. Li-ion batteries are unable to meet huge demands of key markets such as transport and grid storage.

The limitations of Li-ion batteries are as follows:

(i) The energy storage capacity or usable capacity (energy density) is inadequate and unable to utilize full theoretical capacity

(ii) The performance at high C-rate (Power density) is unsatisfactory, especially for the intended applications such as HEVs

(iii) The charge-discharge efficiency (coulombic efficiency) is poor due to large polarization losses and the same is aggravate at higher current rates

(iv) Poor performance at lower temperatures (below 30 °C)

(v) The price is high due to expensive transition metals used in cathode composition

(vi) The safety is a concern due to thermal runaway caused by the exothermic reactions between electrolyte and electrode materials.

1.3 Beyond Li-ion battery

The biggest challenges today confronting complete electrification of automotive industry is simply an energy density of the battery. The need for developing a cost-effective, safe, and long-lived battery with enough energy storage (both in terms of volume and weight) for electrifying transportation sector is ever growing. Based on the electrochemistry and the electrode materials used, conventional Li-ion batteries impose limitations on the energy density that can be achieved. These shortcomings have stimulated research in alternative chemistries labelled beyond lithium ion batteries. New technology in electrochemistry with newer electrode materials that has higher energy densities should be used to go beyond Li-ion batteries.

Among various alternative battery technologies, Li-S and Li-O_2 battery chemistries are promising due to their high theoretical energy density of 2567 and 3505 Wh/Kg respectively (Figure 1-2). Though the basic chemical reactions are different for these battery systems, their cathode materials S and O_2 belongs to same group in the periodic table. Li-O_2 is pre-mature technology and poor oxygen reduction/oxidations makes more complex in nature, therefore it needs fundamental breakthrough in order to obtain promising results. In the other hand, Li–S has been investigated since the 1940s and extensive efforts have been made to address issues related to intermediate polysulfide reversibility reactions over the intervening 70 years

[7]. Moreover, lithium-sulfur (Li-S) system is a promising electrochemical energy storage technology due to following reasons [8-10]

(i) Sulfur cathode has high theoretical capacity of 1674 mAh/g (10X higher than Li-ion battery)

(ii) Sulfur is non-toxic, naturally abundant and renewable

(iii) Cost-effective (byproduct of many industrial processes like oil and gas industry)

(iv) Li-S battery uses high boiling point liquid electrolytes, which is safer than any other Li-ion battery configurations.

Figure 1-2 Practical specific energies for some rechargeable batteries along with estimated driving distances and pack prices[11].

With these promising features, the technology has gained immense and increasing attention over a period of time to reach meet future the energy demands.

1.4 Fundamental chemistry and working principle of Li-S cell

Li-S batteries are the desirable option to go beyond the horizon of Li-ion batteries, because sulfur together with lithium, supporting the electrochemical redox reaction of $16Li + 8S \Leftrightarrow 8Li_2S$ corresponds to the highest theoretical capacity of 1675 mAh/g *vs.* lithium (Figure 1-3). Besides the popularly known advantages of sulfur such as availability of abundant resources, low cost and

low toxicity, added advantages of using sulfur as a cathode for batteries includes intrinsic protection mechanism from overcharging, which enhances battery safety and a wide operating temperature range.

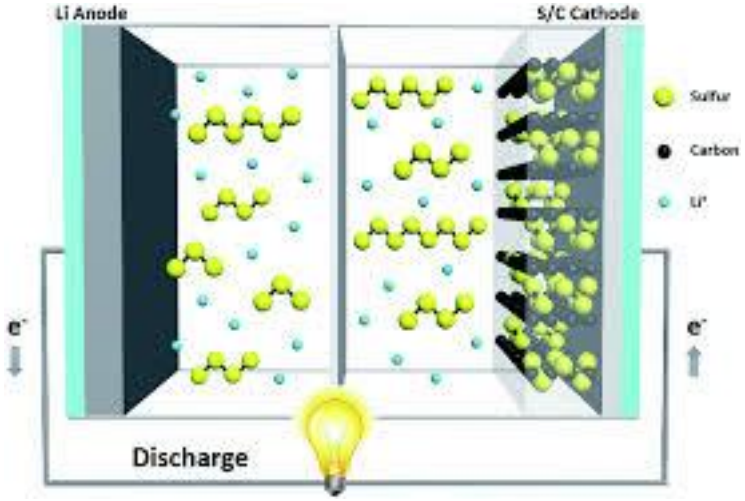

Figure 1-3 Basic working principle of Li-S battery[12]

In Li-S battery, the electrochemical reduction of sulfur during discharge and the oxidation of the products during battery charge occur in two stages. This scenario is evidenced by the shape of discharge and charge curves (Figure 1-4): each shows two plateaus. The first discharge stage of a sulfur electrode, which occurs in the potential range of 2.5–2.0 V, involves the reduction of the elementary sulfur octet dissolved in the electrolyte to lithium octa-sulfide, which is soluble in electrolytes. Lithium octa-sulfides are unstable in electrolyte systems and undergo disproportionation with continuous electrochemical reductions. In a simplified form, the reduction of the elementary sulfur octet can be described by equations (1) and (2).

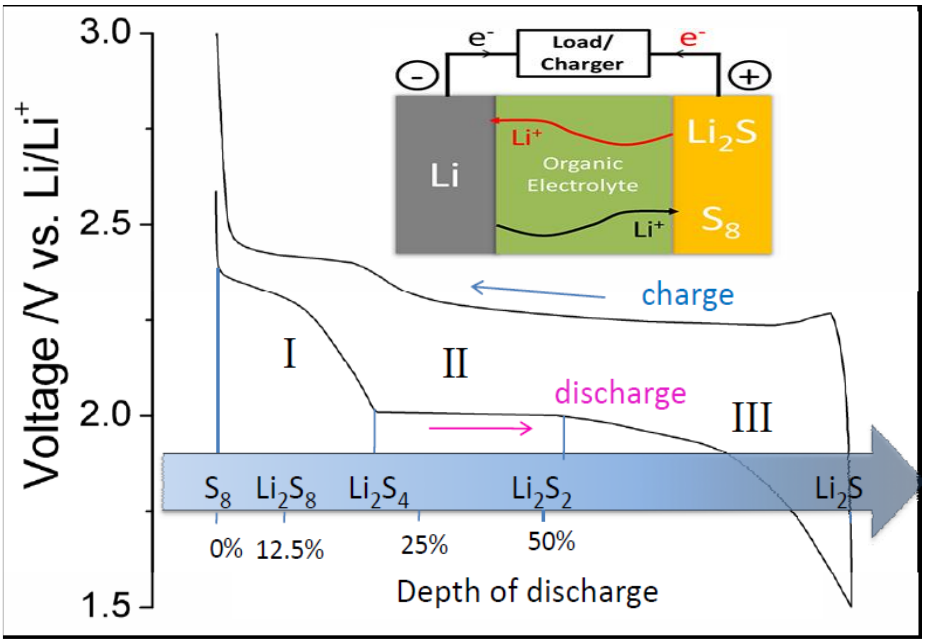

Figure 1-4 Representative charge/discharge behaviour of Li-S batteries[13]

$$S_8 + 2e^- + 2Li^+ \rightarrow Li_2S_8 \text{.....(1)}$$

$$Li_2S_8 \rightarrow Li_2S_n + (8\text{-}n)S \text{.....(2)}$$

The reduction of elementary sulfur to lithium polysulfides is much more complex, however, V. S. Kolosnitsyn and E. V. Karaseva [14] suggests the following possible schemes:

I. The reduction of polysulfide sulfur with a systematic decrease in the polysulfide chain length and the retention of the overall lithium polysulfide concentration in the solution

$$Li_2S_n + 2e^- + 2Li^+ \rightarrow Li_2S\downarrow + Li_2S_{(n-1)} \text{.....(3)}$$

$$Li_2S_{n-1} + 2e^- + 2Li^+ \rightarrow Li_2S\downarrow\ Li_2S_{(n-2)} \text{.....(4)}$$

$$Li_2S_2 + 2e^- + 2Li^+ \rightarrow 2Li_2S\downarrow \text{.....(5)}$$

II. The reduction of polysulfide sulfur as a result of the rapid disproportionation of Li_2S_n with the polysulfide chain length could be retained but with a systematic decrease in the overall lithium polysulfide concentration in the electrolyte solution.

$$Li_2S_n + 2e^- + 2Li^+ \rightarrow Li_2S\downarrow + Li_2S_{(n-1)} \text{.....(6)}$$

$$xLi_2S_{n-1} \rightarrow Li_2S\downarrow + yLi_2S_n \text{.....} \quad ...(7)$$

The actual mechanism of the electrochemical reduction of lithium polysulfides is more complex, likely the first or second mechanism can be implemented depending on the composition of the electrolyte system.

The charge of lithium-sulfur batteries will also occur in two stages, short – chain lithium polysulfides are transformed to long chain ones. The proposed scheme of this process can be represented by:

$$mLi_2S_k - 2e^- - 2Li^+ \rightarrow gLi_2S_n \text{……} (8) \quad \text{where m k=g n}$$

At the end of this process is over, long-chain polysulfides are reduced to elementary sulfur in the potential range 2.4 ~2.6 V *vs.* Li/Li^+

$$mL_2Sn - 2e^- - 2Li^+ \rightarrow (m-1)Li_2S_{n-k} + S\text{…..}(9) \quad \text{where } (mn)=(m-1)((n-k)+1)$$

The viscosity of electrolyte solutions also increases with increasing lithium polysulfide concentration. So, interplay between the adjusting of viscosity of electrolyte and polysulfide concentration requires an attention.

1.5 Current issues, recent developments and deployment challenges in Li-S batteries

However, practical applications of the Li-S battery is hindered by a multitude of issues like short cycle life, poor columbic efficiency, poisoning of Li-anode, self-discharge etc. [15]. The underlying primary reason behind these performance barriers is the well-known polysulfide-shuttle mechanism, a process initiated in the preliminary stages of battery discharging. This mechanism results in dissolution of polysulfides (PS) into the electrolyte solution causing undesirable mass transport of electroactive species resulting in the formation a passivation layer on Li-anode[16]. Herein, all three materials such as cathode, anode and electrolyte are contributing partially to poor performance of Li-S battery. Therefore, it is important to understand the

fundamental problems corresponding to individual components and their possible remedies to realize most celebrated high energy density of Li-S battery.

1.5.1 Cathode: Designing various porous materials to limit polysulfide shuttle process

The sulfur electrode is strongly believed where most of the issues originates and is the key to improve Li-S battery performance. The issues of sulfur cathode as follows

- The poor electrical conductivity of sulfur (5×10^{-30} Scm^{-1}) and its discharge products
- Dissolution of intermediate lithium polysulfides (LiPS) in the electrolyte and deposition on Li anode during 'polysulfide-shuttle process'
- The formation of insoluble low chain irreversible polysulfide products (Li_2S_2 and Li_2S) leads to the increase of cell resistance which increase the polarization difference between charged and discharge potentials. This will further results in the reduction of the columbic efficiency
- Relatively low density (2.07 g cm^{-3} for a sulfur and 1.66 g cm^{-3} for Li_2S)
- The volume expansion of the S cathode during charging and discharging causes pulverization which leads to collapsing of the interconnections and further reduction in the electrical conductivity with the current collector, which causes an increase rate of the capacity fade upon cycling.

To tackle the above mentioned challenges, majority of recent research efforts have been directed towards confining sulfur into pores of carbon materials for improving conductivity of sulfur and trapping intermediate polysulfides with the cathode of the cell [17, 18]. The following are few important contributions in this regard with promising results are discussed.

The research in Li-S battery re-ignited with pioneering work from L.F. Nazar groups on developing highly ordered nanostructured carbon-sulfur cathode [19]. The specific capacity has found to be

enhanced because of the overall improvement in the electrical conductivity of the electrodes. Figure 1-5 shows the mesoporous carbon for sulfur encapsulation with tunable pore sizes and pore volumes. Mesoporous carbon with a relatively larger pore diameter can accommodate higher sulfur loading under optimized filling conditions.

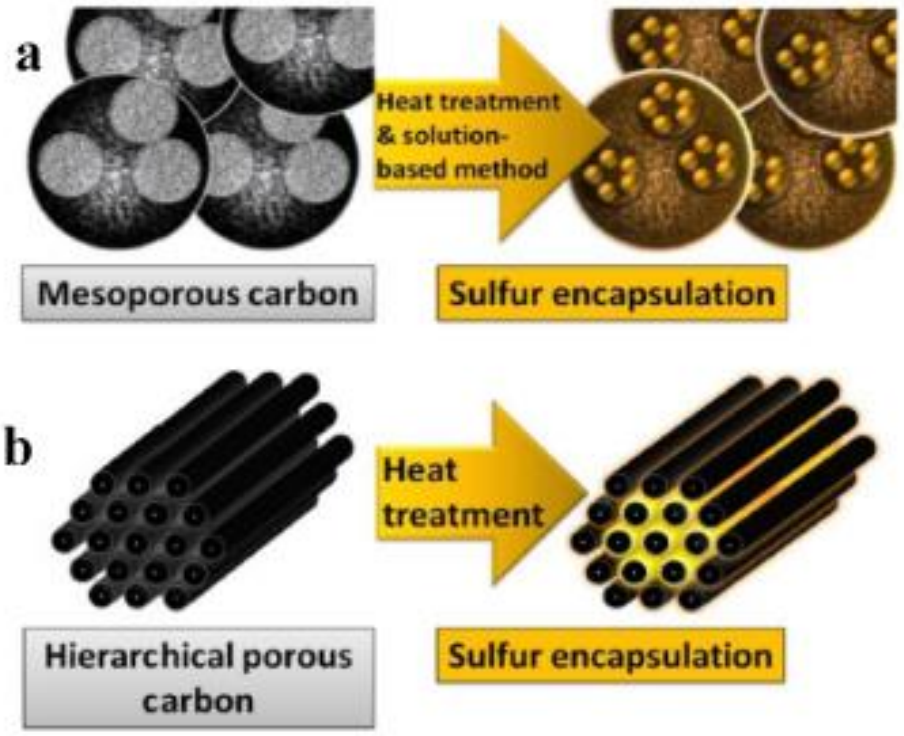

Figure 1-5 Schematic models of a representative a) mesoporous carbon and b) microporous carbon with S as composite electrode [20, 21]

The partial sulfur-filling in these structures have results in limited dissolution/diffusion of polysulfides and ensure a steady electrochemical performances. By using a pore size of 22 nm and with 50% sulfur loading, mesoporous carbon delivered the specific capacity as high as 1390 mAh/g with continuous capacity fade for 100 cycles. The observed high specific capacity was attributed to the highly ordered nano-sized mesoporous structures and the impregnation of sulfur in them.

However, the limitations in achieving high sulfur loading and complexity in designing desirable pores leads to difficult for practical applications.

The two-dimensional (2D) graphene nanosheets were proved to be a promising due to its high specific surface area (2610 m^2/g), unique electronic properties, tunable pore volume and their distribution, and their readily available sites for functionalization with sulfur.

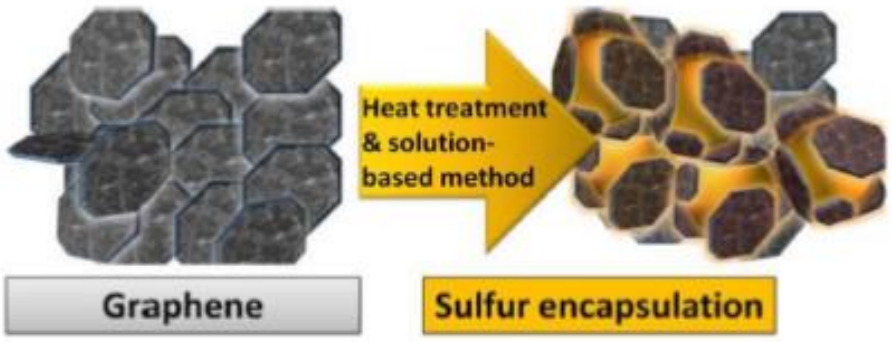

Figure 1-6 Schematic representations of graphene nanosheets for sulfur loading to use as Li-S battery cathode [22].

The possibility of limiting polysulfide shuttle process by tuning surface area of graphene or its composites has also been attempted. Sulfur was impregnated in between graphene layers in the recent report by Wang *et al.* [23]. Though, as prepared nanocomposite showed a capacity of 1505 mAh/g for the first few cycles, severe capacity fade was observed over extended cycles. In other study, it has been used three-dimensional sandwich-type architecture with a layer of graphene sheets/stacks and a layer of sulfur nanoparticles (Figure 1-6). As a result, 52% capacity retention was achieved by such graphene sulfur composite for about 50 charge-discharge cycles.

Bin *et al.* used a simple electrochemical assembly strategy to vertically aligned sulfur−graphene (S-G) nanowalls into electrically conductive substrates [24]. The graphene arrays perpendicularly to the substrates were intended to facilitate the fast diffusions of both lithium and electron, easy access of electrolyte and accommodate of the volume change of sulfur (Figure 1-7).

A high reversible capacity of 1261 mAh/g was observed [24], however, the limited sulfur loading in this composite limit its practical applications.

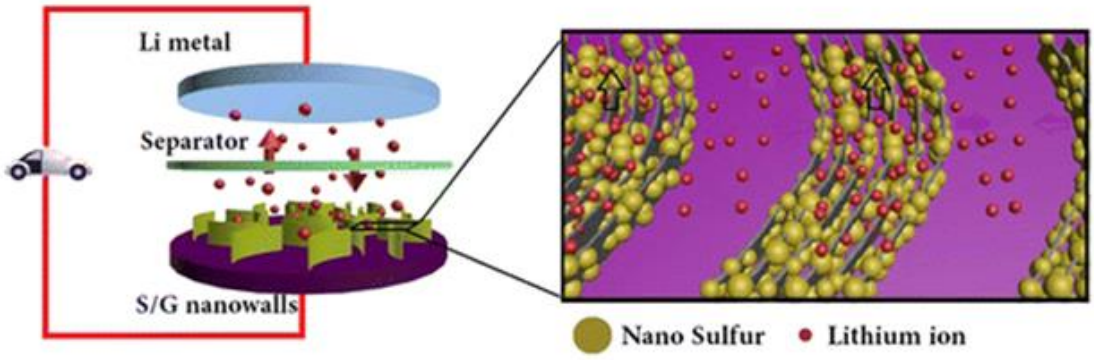

Figure 1-7 Vertically aligned sulfur−graphene (S-G) Nanowalls [24].

Following these studies, there have been wide variety of graphene materials and its derivatives have been used to achieve high sulfur loading in the composite. Some of them have been tabulated carefully in the Table 1-1

material	S content	method	electrolyte (binder)	performance
sulfur−graphene nanosheets	22/18	heat treatment	LiTFSI in PEGDME 500 (PVdF)	600 mA h g^{-1} (40th cycle, 0.03C)
Nafion-coated FGSS	72/57	heat treatment	LiTFSI in DOL + DME (PVdF)	960 mA h g^{-1} (100th cycle, 0.1C)
sulfur−polyacrylonitrile−graphene composite	47/38	heat treatment	$LiPF_6$ in EC + DMC (PTFE)	1200 mA h g^{-1} (50th cycle, 0.1C)
sulfur−graphene oxide composite	66/46	heat treatment	LiTFSI in PYR14TFSI + PEGDME (−)	954 mA h g^{-1} (50th cycle, 0.1C)
CTAB-coated sulfur−graphene oxide composite	80/56	heat treatment	LiTFSI in PYR14TFSI + DOL + DME (SBR/CMC)	740 mA h g^{-1} (1500th cycle, 0.02C)
graphene/PEG-wrapped sulfur	70/56	solution-based method	DOL + DME (−)	550 mA h g^{-1} (140th cycle, 0.5C)
graphene-enveloped sulfur	87/78	solution-based method	LiTFSI in DOL + TEGDME (−)	550 mA h g^{-1} (50th cycle, 0.2C)
sulfur−hydroxylated graphene composite	50/40	solution-based method	$LiCF_3SO_3$ in DOL + DME (PVdF)	1021 mA h g^{-1} (100th cyde, 0.5C)

[a]The sulfur content is presented as S concentration in the composite/S concentration in the electrode (wt %).

Table 1-1 Tabulated graphene-sulfur composites with electrolytes systems and their electrochemical performance [25].

Recently, several polymers have been used to prevent polysulfide shuttle process, especially special attention has been paid for conductive polymers such as polypyrrole, polyaniline, poly(3,4-(ethylenedioxy)thiophene) (PEDOT), etc. (Figure 1-8). Polymers are expected to act as a physical barrier for migration of dissolved polysulfides towards anode. Xiao *et al*. [26] utilized self-assembled PANI nanotubes for sulfur encapsulation, as shown in Figure 1-8a. The PANI nanotubes were treated at 280 °C with sulfur, which resulted in a partial reaction of sulfur with the polymer to form a 3D, crosslinked, structurally stable S−PANI composite. Such a composite delivered a specific capacity of 432 mAh/g at a 1C rate over 500 charge-discharge cycles. The polymer layer is not only rigid and stable but also ionically and electronically conductive, which can effectively block the dissolution of polysulfides and provide pathways for ions.

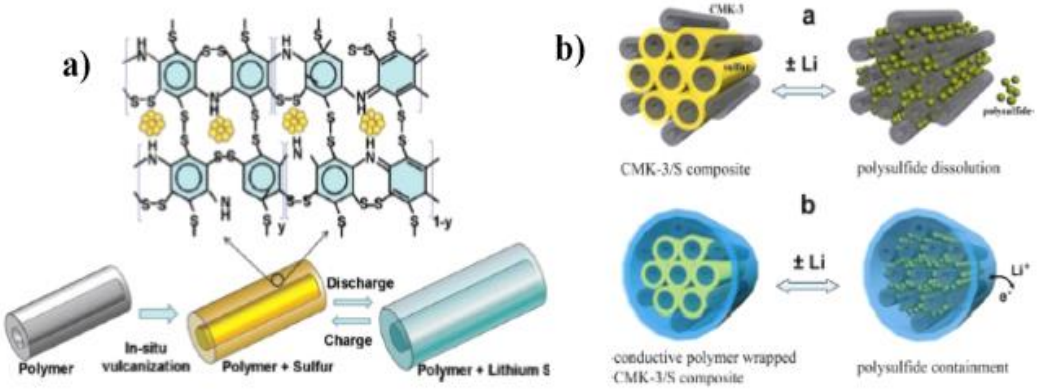

Figure 1-8 Schematic representation of conductive polymer-sulfur composites a) construction of polyaniline-sulfur nanotubes[26] and b) PEDOT/PSS-coated CMK-3−sulfur

Even though, several carbonaceous or conducting polymer materials have been extensively used as electronic conductors for sulfur composites, problems of processing nano/micro porous carbons, binders and achieving high sulfur loading have not yet been thoroughly addressed [28-36]. In spite of some success on effective sulfur loading in some of these porous materials,

dissolution of polysulfides into the electrolyte solution is unavoidable due to their sulfifobic nature. This is because of poor adsorption capability of polysulfides on these non-polar materials and results in undesirable mass transport of electroactive species towards Li-anode [16]. In this regard, Barchasz *et al.,* [37]and others [38-41] reported that passivation of cathode surface by insoluble by-products and poor adsorption of soluble polysulfides are predominant sources for poor electrochemical performance of Li-S battery [42].

Besides these modifications of cathode materials towards improving Li-S battery performance, researchers at Wayne State University have developed a novel approach which highlights the electrocatalytic effect on lithium polysulfide (LiPS) red-ox reactions [43]. Use of electrocatalytic porous current collectors have proven to enhance the reaction kinetics of LiPS due to their catalytic nature and also traps intermediate LiPS due to their porous nature. Further, this electocatalytic approach completely eliminates use of carbon in the Li-S battery configuration. Such elimination of carbon layer in the Li-S battery configuration has not only reduces the burden of making stable electrode (by choosing appropriate binders, additives and solvents), but also significantly enhances the volumetric energy density of the cell [28, 44]. As illustrated in Figure 1-9, the use of electrocatalytic current collectors in Li-S battery configuration has several advantages over conventional carbon based systems, as entire polysulfide shuttle reaction is confined to the surface of porous electrode. High catalytic activity, high surface area, strong affinity towards adsorption of intermediate polysulfides and structural stability towards volume changes in the system are believed to be driving characteristics for better performance of Li-S battery. Conventional electrocatalysts such as nickel (Ni) and platinum (Pt) in the form of thin-film configuration has shown a stable capacity, rate capability and high coulombic efficiency in Li-S battery. Despite the fact that surface chemistry of metal thin-films enhances the PS anchoring

strength, achieving high active material loading is limited due to constrained surface area. Hence, there is clear research opportunity to enhance surface area of electrocatalyst and also find an alternative electrocatalysts that are efficient in enhancing PS shuttle process and cost effective.

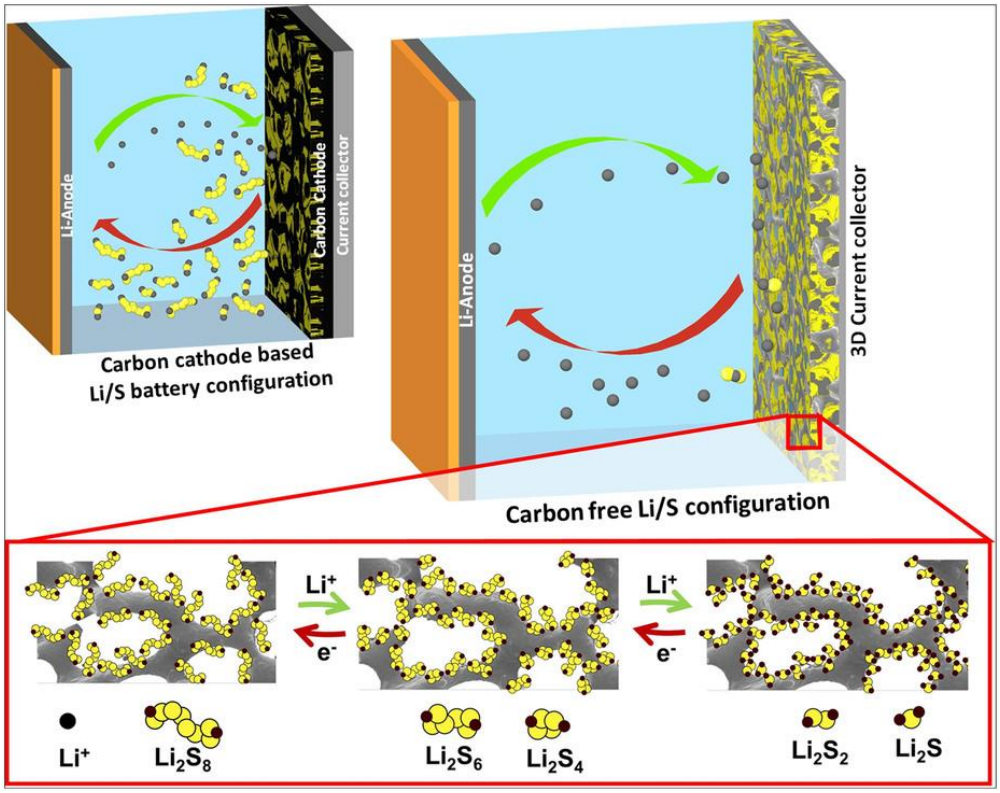

Figure 1-9 Novel electrocatalytically active current collectors containing Li-S battery configuration with PS shuttling mechanism confined on the surface of three dimensional current collectors [43]

1.5.2 Anode: Protection of Li anodes from polysulfide deposition

The stability of anode with electrolyte and dissolved polysulfides determines the long-term cycle life and practical viability of Li−S batteries. Principally, Li-S battery uses metallic lithium as anode due to its low electrochemical potential and high specific capacity. However, use of Li metal negatively influence the cycling stability and safety of rechargeable lithium batteries due to formation of dendrites and unstable passivation layer, known as solid electrolyte interface (SEI layer) on the metallic lithium anode. Apart from dendrite formation, Li-S battery anodes also

suffers from deposition of dissolved sulfide species that diffuses in the electrolyte through the separator. Upon extended charge-discharge cycles, it is often found that the lithium anode became coated with these polysulfides. Hence, there have been several attempts to prevent the deposition of these polysulfides directly on Li-metal surface either in the form of coating a protective layer externally or by introducing additives in the electrolytes that can lead to insitu formation of form passivation layer on Li surface[45].

Silicon with its high theoretical capacity of 3579 mAh/g ($Li_{15}Si_4$) has been considered as a promising alternative for metallic lithium as an anode for Li−S batteries. Silicon nanowires were configured with Li_2S/mesoporous carbon composite cathodes [46] and microspheres of Si/C anodes in combination with S/C cathodes [47]. Similar to Si, Sn–C–Li alloy has also been attempted to replace Li metal. Functional full cell Li-S battery has been fabricated with Sn–C–Li alloy as anode, Li_2S/C cathodes across the gel polymer electrolyte, a polyethylene oxide/Li trifluoromethanesulfonate (PEO/$LiCF_3SO_3$) polymer matrix [48]. Further, Li–Al, $Li_{2.6}BMg_{0.05}$, Li_5B_4, Li_3Mg_7 etc., alloys have also been investigated as a potential anodes to replace metallic Li anodes [49].

On the other hand, protecting the Li metal anode using polymer coatings and additives has also been under intense investigation. Solid polymer electrolytes with good Li^+ conductivity have been employed as a protective layer of Li anodes. Some methods like UV cured polymerization seem to result in smoother and denser surface morphology [50], but due to sluggish Li^+ transport through polymer electrolytes they have resulted in low power density and discharge capacity at room temperature. Apart from the polymer electrolytes to protect Li anodes, it has been reported that polysulfides can be controlled by depositing sulfur powder on Li anodes [51]. Also, additives in electrolytes such as $LiNO_3$ have been found to stabilize the SEI layer on a Li anode [52].

1.5.3 Electrolytes: Modification of electrolytes with additives

A few electrolyte additives have been studied for improving the Li-S cells performance. The expected advantages of having additives in the electrolyte include: (1) protecting Li anode from dissolved PS attack, (2) enhancing the LiPS solubility and stability during charge-discharge process and (3) reducing the viscosity of the liquid electrolyte intern to improve ionic conductivity. Among several additives explored, lithium nitrate salt found effective due to its oxidative nature which enables the Li metal to form a very favorable surface layer, [53] and addition of P_2S_5 is found to promote the dissolution of polysulfides and protect the Li anode, which led to an increase in the capacity retention of the Li-S cells.[54] However, the dissolution of these additives in electrolyte has found to influence cell resistance due to formation of protective insulating layer on electrode and also due to increase in viscosity of electrolyte. Further, artificial interface formed by additives gradually consumed on the Li anode upon long cycling, which leads to a decrease in the protection efficiency. Hence it is important to understand effect of these additives on structural and morphological properties of electrode and formed SEI layer [55].

CHAPTER 2 SCOPE OF THE WORK AND MOTIVATION

2.1 Statement of the problem

Li-ion batteries have been at the forefront in the energy supplying for handheld electronics as well as electric vehicles, however, if the future energy needs are taken into account the current pace of technological progress will be unable to sustain the demand. The limitations on their energy storage capability stimulated the researchers to look for alternate battery technology – Lithium Sulfur batteries (Li-S). Li-S system is a promising electrochemical energy storage technology due to its low cost, high theoretical energy density, safety, wide temperature range of operation and eco-friendliness.

However, practical applications of the Li-S battery are hindered by a multitude of issues like short cycle life, poor columbic efficiency, poisoning of Li-anode, self-discharge etc. The major challenges in lithium sulfur batteries that prevent them of taking a lead role in automotive technology:

1. Poor electronic conductivity of sulfur (10^{-24} S/cm) and the formation of partially reversible discharge products (Li_2S and Li_2S_2) will cause poor reaction kinetics and influence overall redox reaction.
2. High volume expansion due lithiation of sulfur: Starting from solid sulfur all the way to Li_2S at the end of discharge process will cause the sulfur volume increase by 4 times which will affect the physical structure of the sulfur carbon composites as well as the surface electron interface layer between the electrode and electrolyte[56, 57].
3. High solubility of the sulfur into the electrolyte and generation of various soluble polysulfide Li_2S_n ($3 \leq n \leq 6$) intermediates, results in shuttle mechanism. The diffused polysulfide ions have the ability to react directly with Li metal anode causing a formation

of a dendrite which will lead to depletion of the Li-S battery performance. The more polysulfide diffused in the electrolyte the less the columbic efficiency of the battery.

4. High electrochemical polarization of sulfur. Polarization effect is a great challenge for Li-S as well as other battery technologies. It represents the difference between the average charging and discharging voltages. Poorly controlled Li/electrolyte interface, which is responsible for cell polarization upon cycling.
5. Low sulfur utilization during cycling: Since the discharge process in the Li-S system is a chemical conversion reaction, thus all sulfur atoms should react to reach the theoretical capacity. However, because of the poor conductivity of sulfur, it is impossible to reach the theoretical capacity of sulfur.

2.2 Hypothesis and objectives of proposed research

The above mentioned problems like poor conductivity of sulfur and its discharge products, the Li_2S induced volume expansion, polysulfide intermediate's dissolution inspired us to look for new catholyte type cells, in which the overall redox reaction is primarily driven by the dissolution of polysulfides in the electrolyte[58]. Similar to solid C-S composite based cathode configurations, liquid cells based polysulfides have also utilized several carbon matrix, graphene, conducting polymer etc., to trap these polysulfides. However, the poor adsorption of hydrophilic polysulfides into hydrophobic carbons matrix along with poor conductivity associated with end products motivates to find alternative host materials. Recent studies from our group shows enhancement in electrochemical performance of these liquid cathode based system (lithium polysulfides as starting materials) when catalytically active thin-film metals are used [43]. Strong affinity towards polysulfides adsorption along with efficient electron transfer makes Pt and Ni thin film electrodes promising alternatives to conventional carbons. However, the constrained surface area of this novel configuration limits the loading of active material onto it. Thus the need of easily accessible

electrocatalytic system is of great demand to explore this new concept of electrocatalytically driven high performance Li-S batteries. Also, the highly conducting matrix ensures the availability of high surface area to host the polysulfides. Thus to utilize the synergetic effect of catalytic properties and high surface area, developing tailored architectures is a necessary step.

Thus, the present aimed at effectively utilizing catalysts like Pt and Ni by dispersing on high surface area and conductive materials like graphene and also investigating alternative cost-effective catalyst for polysulfide redox reactions. The high surface area, superior mechanical and electrical properties, electrochemical compatibility and its prior attempts to host sulfur cathode, makes graphene as an ultimate choice for supporting electrocatalysts [59-61]. We hypotheses that when the electrocatalyst embedded in high surface graphene and used as cathode for Li-S batteries, the improved electrochemical performances can be easily achieved. The conventional metal catalysts like Pt, Ni can be used to prove the concept and later on can be replaced by easily available cost effective electrocatalyst such as sulfides and carbides, which are proved to be catalytically active towards red-ox reactions.

Based on the above mentioned hypothesis we formulate following objectives as core focus of this dissertation:

- **Investigation of lithium polysulfide redox reactions by dispersing Pt and Ni nanocatalysts on two-dimensional graphene nanosheets:**

The high surface area, superior mechanical and electrical properties, electrochemical compatibility and its prior attempts to host sulfur cathode, makes graphene as an ultimate choice for supporting electrocatalysts for polysulfide redox reactions [59]. Hence, our objective in this regard is to functionalize metal nanoparticles graphene nanosheets and study the electrochemical properties of metal/graphene composites by fabricating Li-S cells. By understanding the relation

between the physical properties of composites and their electrochemical properties, better electrocatalyst/graphene configurations will be engineered.

- **Investigate non-noble metal based electrocatalyst for lithium polysulfide redox reactions:**

Most of the conventional electrocatalysts are either noble metals or composites of them. Identifying an effective electrocatalysts alternative to expensive noble metal based electrocatalysts gains paramount importance in the general field of electrocatalysis. Hence, it is planned to identify suitable and cheaper electrocatalysts towards polysulfide conversion reactions evolved as one of the important objective for this dissertation. Towards this end, transition metal dichalcogenides (TMDs) and metal carbides have been chosen due to their prior attempts as a catalyst in other fields and their known high electrochemical activity similar to most of noble metals. Hence, in this study we propose to synthesize these alternative catalysts in the nanoscale dimensions and investigate their application as potential electrode materials for Li-S battery.

CHAPTER 3 EXPERIMENTAL METHODS

3.1 Important battery terminologies

- **Discharge:** when the battery is connected to external load, electrons start to flow from the anode (oxidation) to the cathode (reduction).
- **Charge**: oxidation occurs in the cathode whereas reduction happens in the anode side
- **Cell potential**: the potential difference between two half cells in a battery, E_0
- **Free energy**: the amount of energy change during the reaction

  $\Delta G^0 = - nFE_0$ where: F is faraday constant (96500 C or 26.8Ah)

  n : number of electrons participated in the reaction

  and E_0: is the standard potential based on the combination of the electrodes
- **Theoretical capacity of the cell**: it depends on the mass of the active material of the cell and the number of the electrons involve in the reaction, where 1 g of an active materials (1gram-equivalent weight=molecular weight of active material divided by the number of electrons involved) will deliver 26.8Ah
- **The C-rate**: the current to discharge the nominal capacity of the battery in 1 hour and it is also the current that is needed for charging or discharging the battery
- **State of charge (SOC)**: gives information about how much charge left in your battery cycle
- **Depth of discharge (DOD)**: is used to describe how deeply the battery is used or discharged. The 100% fully charged battery means the DOD of it is 0%. the battery that delivered 40% of its energy, has DOD equal to 40% and based on that the less the depth of discharged before recharging, the longer the battery will last

- **Open cell voltage (OCV)**: the voltage of a cell when no current is going in or out of the battery and this is measured immediately after battery fabrication
- **Internal resistance (IR)**: the resistance to the flow of the current within the battery.
- **Columbic efficiency**: the ratio of the discharge capacity of the battery to the charge capacity.
- **Specific energy and energy density (Wh/Kg)**: energy delivered by the cell per unit mass or per unit volume.
- **Power density (W/Kg)**: the amount of power per given volume or weight

3.2 Electrochemical techniques

3.2.1 Cyclic Voltammetry (CV)

Cyclic Voltammetry (CV) is an electrochemical technique which measures the current that develops in an electrochemical cell under conditions where voltage is in excess of that predicted by the Nernst equation. CV is performed by cycling the potential of a working electrode, and measuring the resulting current. The potential of the working electrode is measured against a reference electrode which maintains a constant potential, and the resulting applied potential produces an excitation signal. Fabricated cells first scan negatively, starting from a higher potential (normally OCV) and ending at a lower cut-off potential. CV can be used to predict and understand the red-ox reaction in the cell. VMP3 potentiostat (Biologic Science Instrument) was used to perform cyclic voltammetry (CV) studies in the potential window of 1.5-3.0 V at a different scan rates from 0.05 to 1.0 mV/s.

3.2.2 Electrochemical Impedance Spectroscopy (EIS)

By using the electrochemical impedance spectroscopy technique (EIS), information on the electrochemical reactions in the system and transport of reactants/products is obtained. This technique is applied on an electrochemical system which is in equilibrium or under steady state conditions. EIS is based on the application of a sinusoidal voltage (or current) signal on the electrochemical cell. The response of the cell to the sinusoidal perturbation is a sinusoidal current (or voltage), which has the same frequency as the perturbation and is normally shifted in phase. The ratio between the perturbation and the answer is a frequency-dependent complex number, called impedance. Modern instruments to measure impedance spectra are the frequency response analyzers (FRA), commercially available since the 1970's which are directly integrated in the potentiostats [62-63]. An electrochemical system is simulated, using the resistance of the electrolyte, the charge transfer resistance, and the double layer capacitance. The most common representation is the Nyquist plot. The Nyquist plot shows in the x-axis the real part of the impedance and in the y-axis the opposite of the imaginary part of the impedance. It is important that the x-axis and y-axis have the same scale length. The shape of the Nyquist plot is representative of the electrochemical processes at the surface of the electrodes and in the bulk of the electrolyte. It is possible to recognize immediately the resistance of the electrolyte, the resistance of the charge transfer, and other properties of the system. Moreover, the kinetic parameters can be obtained from the plot in the case of simple redox systems. VMP3 potentiostat (Biologic Science Instrument) was used to perform electrochemical impedance studies from 100 mHz to 100 KHz.

3.2.3 Linear Sweep voltammetry

In linear sweep voltammetry, the current at a working electrode is measured while the potential between the reference electrode and the working electrode is swept linearly in time. The experimental setup for linear sweep voltammetry utilizes a potentiostat and three-electrode setup to deliver a potential to a solution and monitor its change in current. Oxidation or reduction of species is registered as a peak or trough in the current signal at the potential at which the species begins to be oxidized or reduced.

3.2.4 Tafel plot

Catalytic reaction parameters can be estimated by plotting logarithm current density *vs* potential, which is known as Tafel plot (Figure 3-1). The slope of the linear region is related to the catalytic activity of the material, which should be low for an efficient catalyst. Exchange current density (i_0) is also related to the reaction kinetics which is determined from the Tafel plot by extrapolating the current density in the linear region [65]. A high i_0 attribute towards the significantly smaller activation barrier which requires a small over potential. The rate of an electrochemical reaction to the overpotential is given by this equation:

$$\Delta V = A\, X \ln(i/io)$$

Where:

- ΔV is the overpotential, V (note that the graph uses η for this quantity)
- A is the so-called "Tafel slope", V
- i is the current density, A/m^2
- i_0 is the so-called "exchange current density", A/m^2

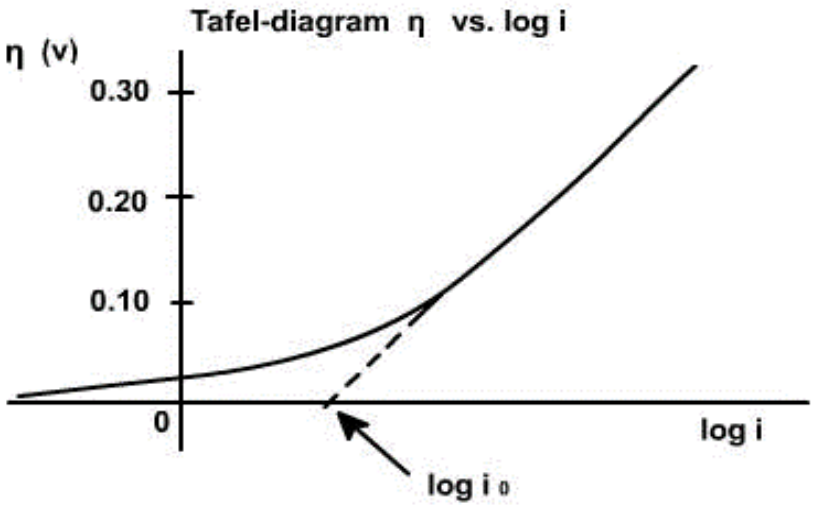

Figure 3-1 Electrochemical potential vs the logarithm of exchange current density.

3.3 Physical characterization techniques [65]

3.3.1 X-ray Diffraction Techniques (XRD)

X-ray diffraction (XRD) has a dual wave/particle nature, which is an effective non-destructive analytical instrument for the analysis of structure, chemical composition and physical properties of different materials. Basically, X-rays are high energy electromagnetic radiation having energies ranging from 200eV to about 1MeV. The interatomic separation in the materials is only a few Angstrom and its corresponding radiation is X-rays. Much of the information about the internal structure of crystals can be obtained by their interaction with X-rays [66, 67]. XRD works based on two basic principles: Bragg's Law and Debye-Scherrer equation

Bragg's law is used to investigate the crystal structure using the equation called Bragg's Equation and it can be mathematically written as:

$$n\lambda = 2dsin\theta$$

where:

n: is integer determining order

λ: is the wavelength

d: is the spacing between the planes n atomic lattice.

$$d_{hkl} = \frac{1}{\sqrt{\frac{h^2}{a^2}+\frac{k^2}{b^2}+\frac{l^2}{c^2}}}$$

where:

a, b, c are lattice spacing of the crystal

h, k, l are Miller indices of the Bragg plane.

θ is angle between incident ray and scattered planes.

Debye-Scherrer equation is used to explain the effect of finite crystallite sizes which is seen as broadened peaks in an XRD. The peak broadening can be due to the size, strain, and instrument. This is applicable if the crystallite size is less than 1000 A^0. By Debbye Scherrer's formula, average grain size (nm) is estimated as:

$$D = \frac{0.9\boldsymbol{\lambda}}{\beta\ cos\theta}$$

Where: λ is the wavelength of CuKα radiation in A^0 units

θ is the angle of diffraction in radians

$$\beta = \frac{FWHM * \pi}{180}$$

β is the Full Width Half Maximum (FWHM) in radians of the XRD peak with highest intensity

From the maximum of recorded diffractograms, lattice parameter (a) and crystallite size can be obtained. Lattice parameter was calculated assuming cubic symmetry and planes were identified by matching with standard values of ICDD.

The main information that can be obtained from a XRD analysis is related to:

▪ Identification of crystalline phase: the space group and unit cell of the crystal structure can be determined by analyzing the peak position and peak intensity of the sample.

▪ Crystallinity: sharp peaks in the diffractogram are related to the crystallinity of the phases. Amorphous phase are present as broad bands.

▪ Crystallite size: the width of the peaks becomes larger when the crystalline size decreases.

▪ Orientation of particles in a sample: preferred orientations of a phase in a sample are related to the relation between the intensity of the ***hkl*** peaks.

X-ray unit used in present study is a fully automated Rigaku Miniflex II X-ray diffractometer using a CuKα source of radiation of λ=1.5418A^{o} at an energy of 8.04 KeV at a scan rate of 0.02°/s. Detection is by ionization and using a Geiger Muller (GM) counter. The arrangement provides for rotation of detector so as to match as that of sample. The use of CuK$_{\alpha}$ radiation minimizes the fluorescence.

3.3.2 Optical Absorption Spectroscopy

Ultraviolet-visible spectroscopy (UV-Vis) deals with the absorption spectroscopy in the ultraviolet-visible spectral region (it uses light in the visible and adjacent (near-UV and near-infrared (NIR)) ranges). In this region of the electromagnetic spectrum, molecules undergo electronic transitions [68]. This technique is complementary to fluorescence spectroscopy, in which the fluorescence deals with transitions from the excited state to the ground state, while absorption measures transitions from the ground state to the excited state. The absorption spectra were collected using Shimadzu UV-3600 UV- Vis- NIR spectrophotometer.

3.3.3 Transmission Electron Microscopy (TEM)

TEM is a microscopic technique where a beam of electrons is transmitted through an ultrathin specimen and interacting with the specimen as it passes through. An image is formed from the interaction of the electrons transmitted through the specimen. This image is magnified

and focused onto an imaging device, such as a fluorescent screen, on a layer of photographic film, or to be detected by a sensor such as a CCD camera.

A TEM is composed of several components, which include a vacuum system in which the electrons travels, an electron emission source for generation of the electron stream, a series of electromagnetic lenses, as well as electrostatic plates. The latter two allow the operator to guide and manipulate the beam as required. Also required is a device to allow the insertion into, motion within, and removal of specimens from the beam path. Imaging devices are subsequently used to create an image from the electrons that exit the system. TEM studies were carried out with a JEOL JEM-2010 instrument.

3.3.4 Scanning Electron Microscope (SEM)

A focused beam of electrons is used to scan the surface of the material to produce images for the samples. When electrons interact with atoms, various types of elastic and inelastic processes occur, including electron scattering and excitation, which produces (1) secondary electrons, (2) backscattered electrons, (3) Auger electrons, (4) characteristic X-rays, (5) bremsstrahlung or continuous X-rays, and (6) photons of various energies, including those in the infrared, visible, and ultraviolet. All the produced signals can be detected to know the information about the sample's surface topography and composition [70]. The electron beam is generally scanned and the beam's position is combined with the detected signal to produce an image. SEM can achieve resolution up to 1 nanometer. Specimens can be observed in high vacuum, in low vacuum, in wet conditions and at a wide range of cryogenic or elevated temperatures. By scanning the sample and collecting the secondary electrons with a special detector, an image displaying the topography of the surface is created.

The fraction of energy deposited by an electron beam in a sample associated with these different processes is dependent on the sample. Secondary and Auger electrons can only be observed when they come from the near-surface region of a solid (typically < 500 Å for insulators, such as silicate minerals, and < 100 Å for metals such as gold). Thus, measurements involving these types of electrons are "surface sensitive". Secondary electrons are generated by the primary electron beam as it enters a sample as well as by backscattered electrons as they exit a sample. Secondary electrons, which typically have kinetic energies < 50 eV, are sensitive enough to differences in surface topology that they can be readily observed from the surface of a sample. Such electrons form the basis of scanning electron microscopy.

3.3.5 Energy Dispersive X-ray Analysis (EDX)

Energy-dispersive X-ray spectroscopy (EDX) is an analytical technique used for rapid qualitative and quantitative analysis of elemental composition with a sampling depth of 1-2 microns. It is one of the variants of X-ray fluorescence spectroscopy which relies on the investigation of a sample through interactions between electromagnetic radiation and matter, analyzing X-rays emitted by the matter in response to being hit with charged particles [71]. Its characterization capabilities are due in large part to the fundamental principle that each element has a unique atomic structure allowing X-rays that are characteristic of an element's atomic structure to be identified uniquely from one another. Morphology (Field emission electron microscopy images) and elemental compositions (Energy dispersive X-ray spectrum) of the prepared samples like graphene composites, carbides and sulfides were studied by JEOL JSM-7500F system operated with accelerating voltage 20 kV in this present study.

3.3.6 X-ray Photoelectron Spectroscopy (XPS)

X-ray photoelectron spectroscopy (XPS) is a quantitative surface chemical analysis technique used to analyze the elemental composition, empirical formula, chemical state and electronic state of the elements in the materials under ultra-high vacuum conditions. XPS spectra are obtained by irradiating a material with a beam of X-rays while simultaneously measuring the kinetic energy and number of electrons that escape from the surface (1 to 10 nm of the material) being analyzed [72]. Also the elemental compositions of the newly prepared nanomaterials are studied using this technique. PHI Quantera X-ray photoelectron spectrometer (XPS) has been used in our studies.

CHAPTER 4 ELECTROCATALYTIC POLYSULFIDE-TRAPS FOR CONTROLLING REDOX SHUTTLE PROCESS OF LI-S BATTERY

4.1 Introduction

Practical applications of the Li-S battery is hindered by a multitude of issues like short cycle life, poor columbic efficiency, poisoning of Li-anode, self-discharge etc.[15]. The underlying primary reason behind these performance barriers is the well-known polysulfide-shuttle mechanism, a process initiated in the preliminary stages of battery discharging. This mechanism results in dissolution of polysulfides (PS) into the electrolyte solution causing undesirable mass transport of electroactive species resulting in the formation a passivation layer on Li-anode [16]. Insulating nature of sulfur and its end products of discharge (Li_2S_2 and Li_2S) further lead to slow charge/discharge process and cell polarization losses [73, 74]. Barchasz *et al.* [37]and others [38-41] reported that passivation of cathode surface by insoluble by-products and poor adsorption of soluble polysulfides are predominant sources for poor electrochemical performance of Li-S battery [42].

To tackle the above mentioned challenges, majority of recent research efforts have been directed towards designing polymer electrolytes that prevents the migration of PS,[75, 76] and surface coatings on Li-anode to avoid PS passivation[77, 78]. In other hand, carbon materials for improving conductivity of sulfur and trapping intermediate polysulfides with the cathode of the cell [17, 18]. In search of finding carbon hosts for polysulfides, several micro/meso porous structures, carbon nanotubes, graphene etc. [30, 33, 79-84] have been investigated thoroughly. The poor adsorption capabilities of carbons towards polar natured polysulfides [85] have further triggered research interest in finding alternative host materials [86, 42, 87-89]. Moreover, the polysulfide conversion reaction kinetics worsens with prolonged cycling due to increase in internal resistance caused by deposition of insulating natured short-chain PS.

In marked contrast to all the above mentioned approaches, we have recently demonstrated that the polysulfide-shuttle process in Li-S cell can be controlled by means of electrocatalysis [43]. Use of electrocatalytic current collectors such as Pt or Ni when coated on Al foil has shown to enhance both cycle life and reaction kinetics (charge/discharge rates) of the Li-S battery [43]. Despite the fact that surface chemistry of metal thin films enhances the PS anchoring strength, active material loading is limited due to constrained surface area. In order to effectively utilize catalysts (Pt and Ni) while ensuring high surface area to host polysulfides, the present study is aimed at understanding structural and electrochemical properties of graphene supported nanocatalyst. The high surface area, superior mechanical and electrical properties, electrochemical compatibility and its prior attempts to host sulfur cathode, makes graphene as an ultimate choice for supporting electrocatalysts [59-61]. We envisage electrocatalyst anchored graphene opening up a new avenue for resolving the host problems associated with Li-S battery.

4.2 Experimental section

4.2.1 Synthesis of metal particles anchored graphene nanocomposites

Graphene flakes were procured from graphene-supermarket and functionalized by refluxing with concentrated nitric acid to decorate metal nanoparticles. In a typical procedure, 1 g of graphene was treated with 50 ml of concentrated HNO_3 and the resulting suspension was refluxed for 7 h and cooled. It was then filtered, washed with de-ionized water and methanol, and dried at 70 °C. To anchor metal (Pt and Ni) nanoparticles on the graphene flakes, $NaBH_4$-assisted polyol reduction was employed. Briefly, stoichiometric amount of metal precursor (H_2PtCl_6 as Pt precursor and $NiCl_2$ as Ni precursor, respectively) dispersed in ethylene glycol solution and functionalized graphene dispersed in ethylene glycol solution were mixed together and taken in a round-bottom flask equipped with a N_2 in/outlet. The pH of resulting suspension was adjusted to

11 by adding 2.5 M NaOH in ethylene glycol and heated to 120 °C. During this process, $NaBH_4$ solution (dissolved in ethylene glycol) was added slowly and refluxed for 3 h. It was then filtered, washed copiously with ethanol, and dried at 70 °C in a vacuum oven. The chemical reactions are as follows:

$$H_2PtCl_6 + 6NaBH_4 + 3CH_2OH\text{-}CH_2OH \rightarrow Pt + 6B\,(OC_2H_5)_3 + 6NaCl + H_2$$

$$NiCl_2 + 2NaBH_4 + 2CH_2OH\text{-}CH_2OH \rightarrow Ni + 2B\,(OC_2H_5)_3 + 2NaCl + H_2$$

4.2.2 Preparation of catholyte

The electro-active species containing catholyte solution (600 mM) for electrochemical properties has been prepared using calculated amounts of Li_2S and S to attain nominal formula of long-chain LiPS (Li_2S_8) in tetraethylene glycol dimethyle ether (TEGDME) at 90 °C for 12h or until all the solid particles dissolves. These molar concentrations are calculated based on the amount of active species i.e sulfur in LiPS solution.

The preparation procedure as follows:

$$0.6*[Li_2S + 7S \rightarrow Li_2S_8] + LiNO_3 + \text{LiTFSI}$$

$$0.6[\frac{Li_2S}{200} + 7\frac{S}{200} \rightarrow \frac{Li_2S_8}{200}] + \frac{LiNO_3}{200} + \frac{\text{LiTFSI}}{200}$$

$$0.6[\frac{45.95}{200} + 7\frac{32}{200}] + \frac{68.95}{200} + \frac{287.1}{200}$$

$0.1378g\ of\ Li_2S + 0.672g\ of\ S + 0.3448g\ of\ LiNO_3 + 1.4355$g of LiTFSI in 5ml of TEGDME.

4.2.3 C-rate Calculation

The C-rate of a battery is a measure of the rate at which a battery is discharged relative to its maximum capacity. A 1C rate means that the discharge current will discharge the entire battery in 1 hour. For a battery with a capacity of 10 A.h, this equates to a discharge current of 10 A. Current needed for constant current discharge in 1 hour , Also called 1-hour rate , C/10 = rate needed to discharge in 10 hours , 3C = rate needed to discharge in 1/3 hour = 20 minutes. The C-rate can be calculated using the theoretical capacity of the sulfur electrode from the following equation:

$$C - Rate(mA) = \frac{1675 * mass\ of\ sulfur(mg)}{1000}$$

Molarity Concentration	0.06M	0.2M	0.6M	0.8M	1M
Mass of sulfur in 10 microliter of PS	0.1513mg	0.513mg	1.53mg	2.048mg	2.56mg
C rate (A)	0.000256	0.000859	0.00256	0.00343	0.00429
C/2 rate(A)	0.000128	0.000429	0.00128	0.00172	0.00214
C/5 rate(A)	0.000051	0.000172	0.00051	0.00069	0.00086
C/10 rate(A)	0.000026	0.000086	0.00026	0.00034	0.00043

Table 4-1 Catholyte concentration, mass of sulfur and corresponding C-rate.

An active material containing catholyte solutions were prepared from stoichiometric amounts of Li_2S and S to form long-chain lithium polysulfides (Li_2S_8) in tetraethylene glycol dimethyle ether (TEGDME) with effective stirring at 90 °C for 12h. The catholyte concentrations used in this study is 0.6, 0.8 and 1.0 M of Li_2S_8 corresponds to 1.21, 1.61 and 2.0 mg of sulfur per cm^{-2} and these are calculated based on the sulfur content in Li_2S_8 and the quantity of catholyte used per cell (10 μl).

4.2.4 Electrode Preparation

Aluminum (Al) foil as a current collector and a routine blade coating procedure is widely used to fabricate Li-S batteries. This traditional battery production process does not allow a high mass loading because a thick electrode tends to delaminate from the Al current collector after coating and drying. Furthermore, the kinetic limitation of lithium diffusion through a thick electrode would induce large polarization and, as a consequence, loss of energy efficiency. The positive electrode was fabricated by mixing graphene and its composites individually with conductive carbon (Super-P) and polyvinylidene fluoride binder in the weight ratio of 80%: 10%: 10%. The mixture was made as slurry using N-methyl-2-pyrrolidone (NMP) as solvent and coated on aluminum foil. The coated electrode was dried in oven at 80 °C to evaporate NMP, and cut into circular discs of 12.7 mm diameter Figure 4-1.

Figure 4-1 25μm the thickness of the electrode

The electrochemical measurements were performed on CR2032 type coin cells containing coated graphene and its composites as working electrodes and lithium metal as counter and reference electrode. Known molar concentration of catholyte used as active material along with an

electrolyte consists of 1 M of lithium bis (trifluoromethanesulfonyl) imide (LiTFSI) and lithium nitrate ($LiNO_3$) in TEGDME and celgard separator. For better comparison, parameters such as concentration and quantity of catholyte (0.6 M and 10 μl) during cell fabrication have been maintained constant. Cell fabrication and assembly is shown in Figure 4-2.

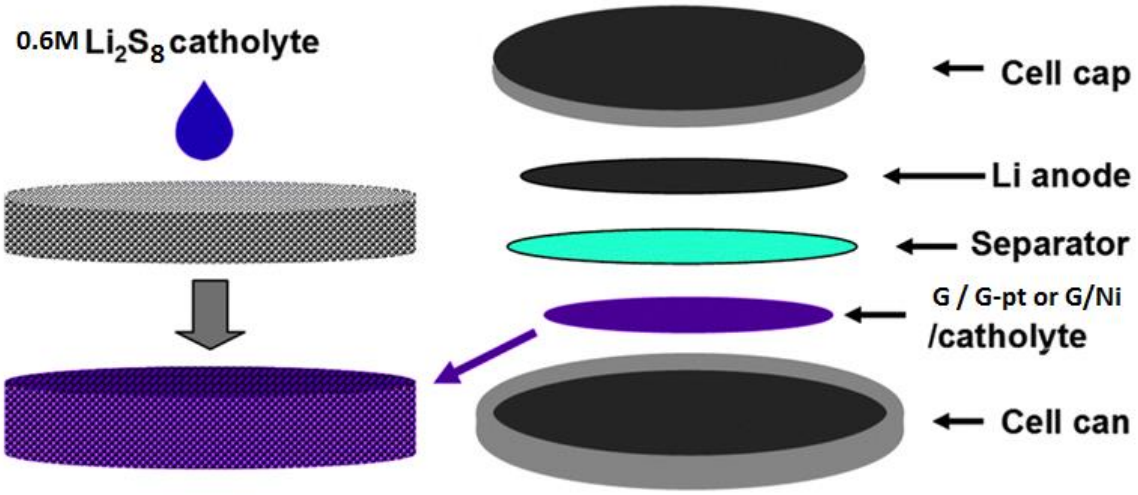

Figure 4-2 Cell assembly configuration

4.2.5 Characterization techniques

X-ray diffraction (XRD) patterns are recorded on a Rigaku Miniflex II X-ray diffracto meter using a CuKα source at a scan rate of 0.02° s^{-1}. Morphology (Field emission electron microscopy images) and elemental compositions (Energy dispersive X-ray spectrum) are studied by JEOL JSM-7500F system operated with accelerating voltage 20 kV. PHI Quantera X-ray photoelectron spectrometer (XPS) has been used to characterize electrodes surface. VMP3 potentiostatic (Biologic Science Instrument) was used to perform cyclic voltammetry (CV) studies in the potential window of 1.5-3.0 V at a different scan rates from 0.05 to 1.0 mV/s. Tafel plots have been obtained from potentiostatic polarization technique. Galvanostatic charge- discharge measurements were performed for composites at different current rates (0.1, 0.2, 0.5 and 1.0 C rate) in the potential range of 1.5 - 3.0 V using ARBIN charge-discharge cycle life tester.

4.3 Results and discussion

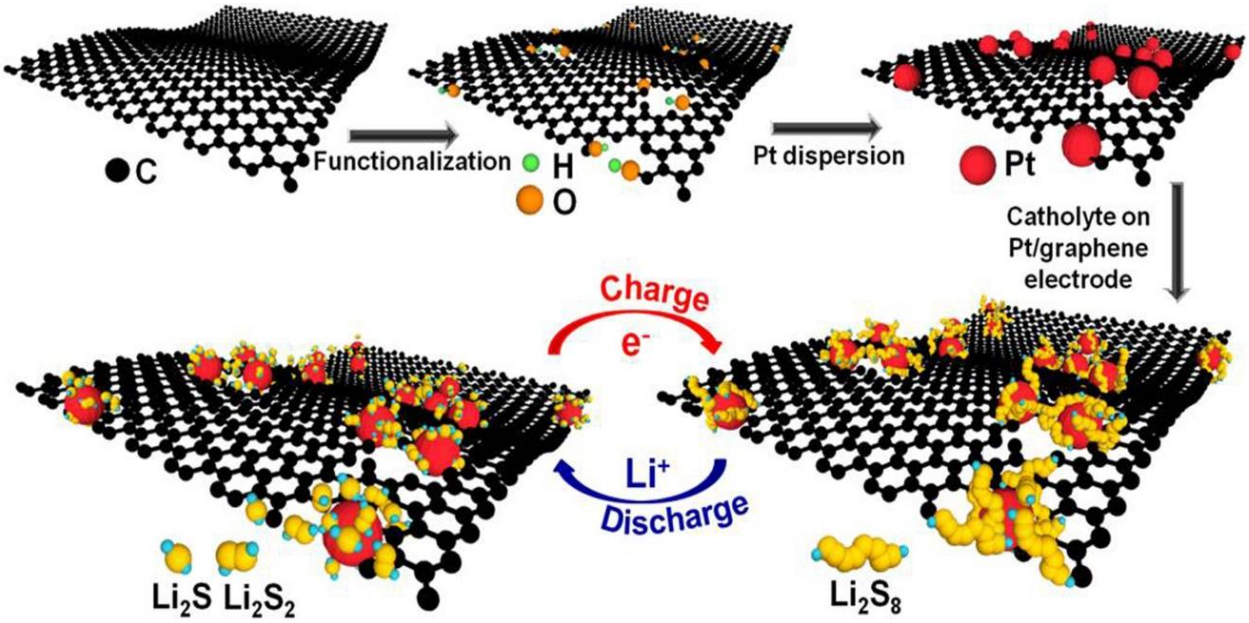

Figure 4-3 Schematic representation of the electrocatalyst anchored graphene naonocomposite preparation and interaction of electrocatalyst-polysulfides during charge/discharge process of Li-S battery

Chemical functionalization of few layer graphene was performed in reflux condenser using concentrated nitric acid at 120 °C under the Argon (Ar) flow. Platinum and nickel nanoparticles are dispersed uniformly on such a functionalized graphene sheets to increase their surface anchoring strength [89, 90]. Step-by-step process of graphene nanocomposites preparation and their interaction with lithium polysulfides during charge/discharge process are illustrated schematically in Figure 4-3.

4.3.1 X-ray diffraction studies

Powder XRD patterns recorded for commercial graphene, functionalized graphene, and metal/graphene in the 2θ range of 20-90 deg. are shown in Figure 4-4. Both graphene and functionalized graphene exhibited a characteristic (0 0 2) diffraction peak at 26.5, corresponding to the interspacing between the graphene layers as 3.34 Å and graphitization degree as 95.3%.

Pt/graphene exhibited five characteristic diffraction peaks at 2θ values around 40, 47, 68, 82, and 87 corresponding to the (1 1 1), (2 0 0), (2 2 0), (3 1 1) and (2 2 2) planes of face-centered cubic (fcc) structure of Pt. Ni/graphene exhibited three characteristic diffraction peaks at 2θ values around 44, 51, and 76 corresponding to the (1 1 1), (2 0 0), and (2 2 0) planes of face-centered cubic (fcc) structure of Ni. Broad diffraction indicated the nano-sized metal crystallites in the prepared metal/graphene materials. Average crystallite size was calculated from Scherrer's equation for the XRD peak assigned to Pt (2 2 0) and Ni(2 2 0). It is determined to be 2.8 and 4.1 nm for the Pt/graphene and Ni/graphene, respectively.

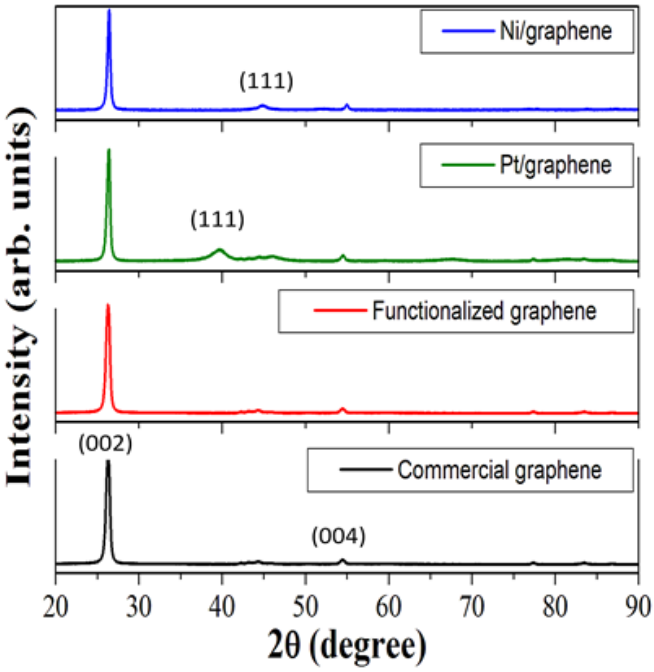

Figure 4-4 Powder XRD patterns recorded for the graphene and metal/graphene composite materials.

4.3.2 Field Emission Scanning Electron Microscopy (FESEM)

Field emission scanning electron spectroscopy (FESEM) images and elemental mapping of Ni/Graphene and Pt/Graphene are shown in Figure 4-5. FESEM images depicted randomly

oriented, transparent graphene sheets of few microns in size and ripple-like flake morphology. In the case of Ni/Graphene and Pt/Graphene composites, a spatial distribution of metallic nanoparticles about 20 nm in size over the layered graphene sheets was observed (Figure 4-5a, b). Further, energy dispersive X-ray spectroscopic (EDX) analysis confirmed the homogeneous distribution of respective elements with (Figure 4-5c, d).

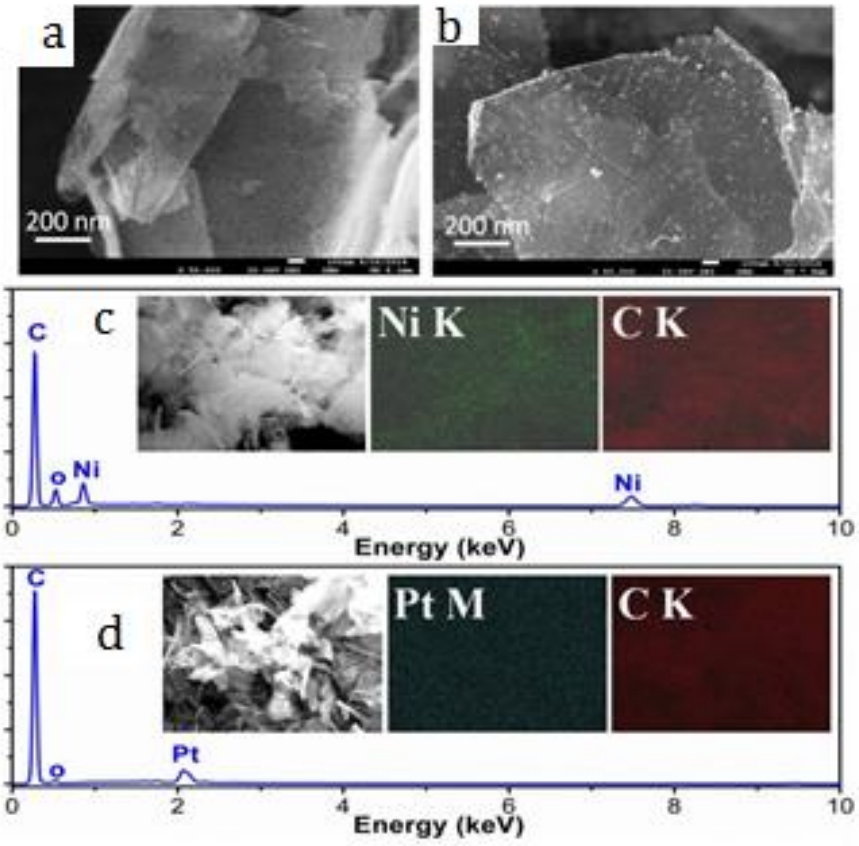

Figure 4-5 Characterization of nanocomposites: (a) and (b) FESEM images (c) and (d) EDX and elemental mapping (inset) of Ni and Pt nanoparticles anchored graphene layers prepared by polyol process respectively.

4.3.3 Electrochemical properties

To evaluate the electrochemical performance of graphene and its nanocomposites, standard 2032 coin cells were fabricated using them as cathode *vs* metallic lithium as an anode and dissolved Li_2S_8 in electrolyte (catholyte) as an active material. For better comparison, parameters such as

concentration and quantity of catholyte (0.6 M and 10 µl) during cell fabrication have been maintained constant. Galvanostatic charge-discharge studies were performed at a constant current rate of 0.1 C (based on sulfur mass in the cell) and obtained results for 100 cycles have been displayed in Figure 4-6. From Figure 4-6a, it has been observed that electrodes exhibited well defined discharge plateaus corresponding to the formation of soluble long-chain PS and their spontaneous dissociation to short-chain PS and vice-versa during charging process. On careful observation, Pt/Graphene electrode shows two discharge plateaus at 2.4 and 1.97 V and a charging plateau at 2.34 V. These features along with reduced polarization at any depth of discharge (DOD) compared to that of pristine graphene electrode is clear evidence for improved PS conversion reaction kinetics.

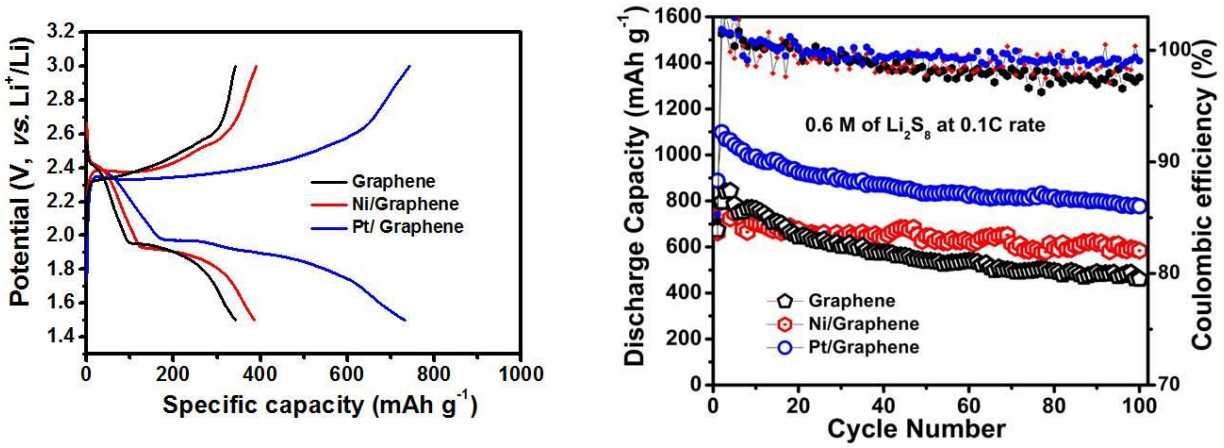

Figure 4-6 Electrochemical performance: (a) voltage vs specific capacity profile and (b) galvanostatic charge-discharge behavior and coulombic efficiency of pristine and electrocatalyt anchored graphene electrodes vs Li^+/Li at 0.1C rate in the potential range of 1.5-3.0 V.

The specific capacity and columbic efficiency of Graphene, Ni/Graphene and Pt/Graphene cathodes with 0.6M of Li_2S_8 (1.21 mg of Sulfur per cm^{-2}) at 0.1 C rate has been displayed in Figure 4-6b. Ni/Graphene and Pt/Graphene electrodes exhibit initial specific capacity of 740 and 1100 mAh g^{-1} and retains a stable capacity of 585 and 780 mAh g^{-1} after 100 cycles of charge/discharge.

In comparison with pristine graphene, Ni/Graphene and Pt/Graphene resulted in 21% and 41% enhancement in capacity respectively. More notably, Pt/Graphene electrode showcases excellent stability in columbic efficiency (~99.3%) upon cycling. The deposition of insulating PS on graphene impedes the electron transfer at electrode/electrolyte interface and results in an increase of internal resistance. In case of electrocatalyst anchored graphene, the presence of catalyst (Pt or Ni) helps to convert these PS deposits back to soluble long chain polysulfides and hence enhances reaction kinetics and retains high columbic efficiency. As Pt/Graphene is found to exhibit superior performance over Ni/Graphene and graphene (Table 4-2), we have further evaluated its electrochemical properties under various conditions such as high current rates, concentrations of PS and temperature of the cell.

	Type of Electrode		
Electrochemical properties	**Graphene**	**Ni/Graphene**	**Pt/Graphene**
Capacity at 100th cycle (mAh g^{-1})	**460**	**580**	**789**
Coulombic efficiency at 100th cycle (%)	**97.3**	**98.2**	**99.0**
Discharge plateau (V)	**1.94**	**1.94**	**1.97**
Polarization difference at 50% of DOD (V)	**0.51**	**0.50**	**0.44**

Table 4-2 Tabulated electrochemical parameters of pristine and electrocatalyt anchored graphene nanocomposite electrodes *vs* Li^+/Li at 0.1C rate in the potential range of 1.5-3.0 V.

Electrochemical behaviour of Graphene and Pt/Graphene electrodes at different C-rates has been performed to reveal the surface anchoring strength of electrocatalyst towards PS conversions. As shown in Figure 4-7a, Pt/Graphene electrode delivers superior specific capacity compared to that of pristine graphene electrode at both C/5 and C/10. For instance, the discharge capacity of 780 mAh g^{-1} has been exhibited by Pt/Graphene electrode at 0.2 C for 100 cycles. This is almost double as that of graphene (380 mAh g^{-1}) under similar conditions.

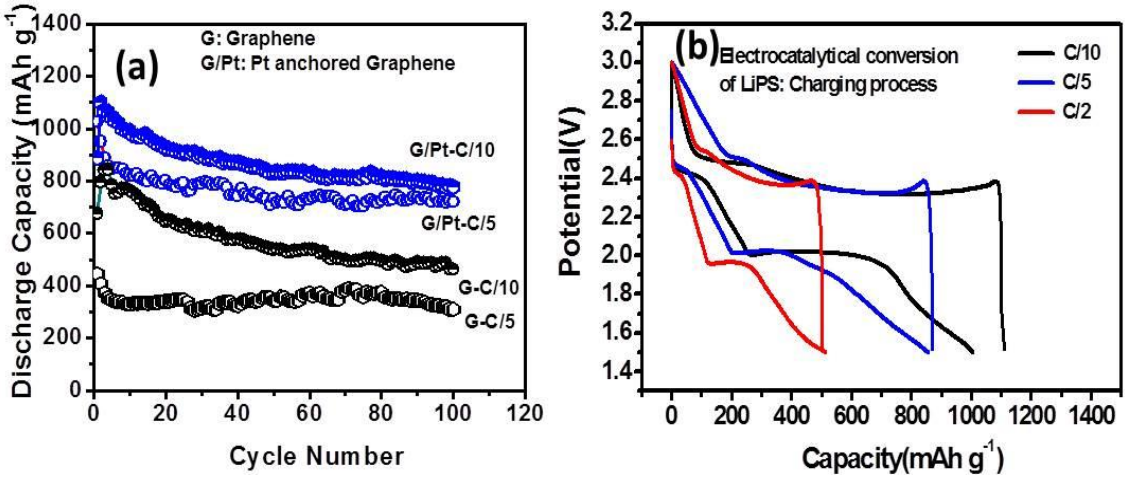

Figure 4-7 (a) Cyclic stability and C-rate tests and (b) corresponding charge-discharge profiles of Pt/Graphene electrodes vs Graphene ones.

Voltage *vs* capacity plot for the Pt/Graphene electrode shows typical discharge and charge plateaus at high current rates (Figure 4-7b). The charging plateau relies more on the electrochemical activity of cathode material which includes conversion of short-chain to long-chain LiPS. The consistency in charging plateaus, even with high C-rates suggests the enhanced reaction kinetics due to presence of electrocatalyst. As Pt/Graphene is found to exhibit superior performance over Ni/Graphene and graphene, we have further evaluated its electrochemical properties under various conditions such as high current rates, concentrations of PS and temperature of the cell. The Pt/Graphene electrode was further subjected to long cycling (about 300 cycles) at 1C-rate and it exhibited a stable performance with minimal capacity loss of 0.09% per cycle (Figure 4-8).

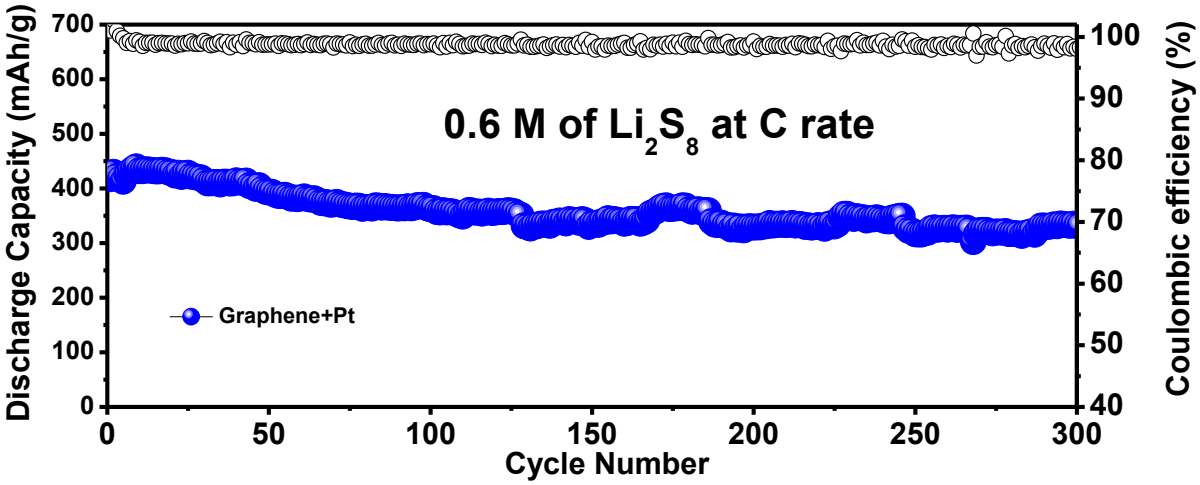

Figure 4-8 Long cycling behavior of Pt/graphene electrode at 1C rate.

In order to validate the electrocatalytic activity of Pt/Graphene over pristine graphene, Cyclic voltammograms (CVs) have been recorded at a slow scan rate of 0.05 mV s^{-1} (Figure 4-9).

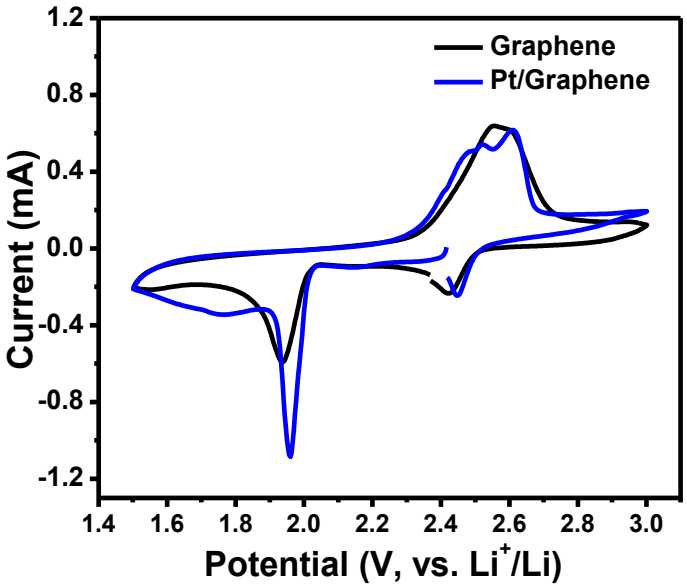

Figure 4-9 Cyclic voltammograms of Graphene and Pt/Graphene electrodes at a scan rate of 0.05 mV s^{-1}

Further, Tafel plots and corresponding exchange current density values have been derived from potentiostatic polarization experiments to understand the effect of catalyst on charge transfer

kinetics during charge and discharge reaction process (Figure 4-10). The calculated exchange current densities (i^0) of pristine and Pt/Graphene electrodes are 1.18 and 3.18 mA cm^{-2} for cathodic process and 0.17 and 0.29 mA cm^{-2} for anodic process, respectively (Table 4-3).

Electrode	$E1_{pa}$ & $E2_{pa}$	$E1_{pc}$ & $E2_{pc}$ (V)	Peak separation ($E1_{pa}$ ~$E2_{pc}$)	Exchange current density (I_0) (mA cm^{-2})
Pristine Graphene	2.57 (broad)	2.42 & 1.93	0.64	1.25 (cathodic) 0.25 (anodic)
Pt anchored Graphene	2.51 & 2.60	2.45 & 1.96	0.55	3.98 (cathodic) 0.40 (anodic)

Table 4-3 . Electrocatalytic parameters for pristine and Pt anchored graphene electrodes are derived from cyclic voltammograms and potentiostatic polarization

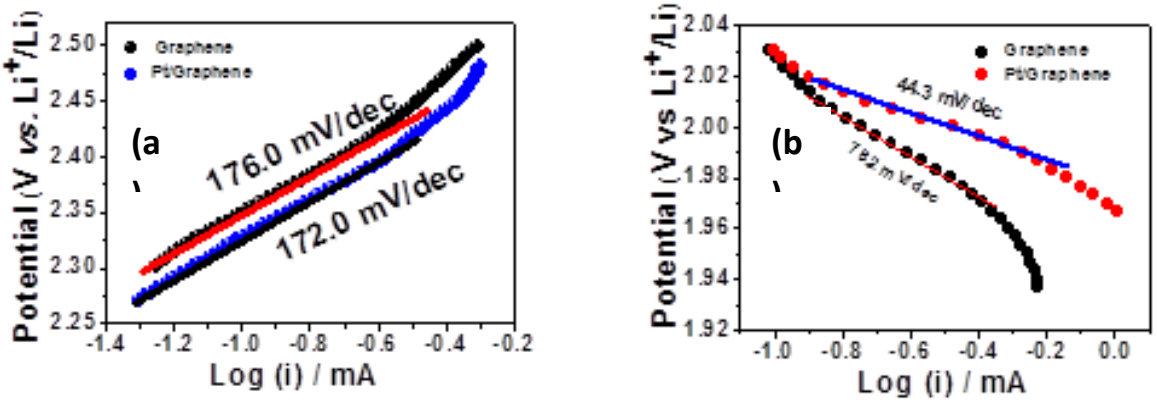

Figure 4-10 Tafel plots for corresponding oxidation and reduction reactions

Thus, the increase in exchange current density values of Pt/Graphene in both charge and discharge process confirms the enhancement in rate of LiPS conversion reactions. During potentiostatic technique, we step down the 10mV step-by-step from OCV to 200 mV for cathodic process; on each potential step current has been recorded with respect to time for 60 seconds. Similarly, electrodes have been discharged completely (up to 1.5 V) and rested for couple of hours to attain the equilibrium state. Such electrodes were polarized by applying step-by-step constant

potential to monitor current with respect to time. Tafel plots have been obtained to derive kinetic parameters from such constant potential steps versus current values at charge-transfer kinetics (after 5 seconds).

Further, electrochemical impedance spectra (EIS) have been recorded to envisage the electrocatalyst influence on charge transfer resistance. Figure 4-11 shows the typical Nyquist plots measured before and after 10 charge-discharge cycles. An inferior electrode-electrolyte interface resistance for Pt/Graphene (60Ω) over pristine graphene electrode (170Ω) has been observed. Furthermore, EIS of pristine graphene exhibits an extra-flattened semicircle, which could be due to deposition of insoluble products on electrode surface. Hence, reduced redox peak separation, higher exchange current density and minimal electrode-electrolyte resistance are clearly in agreement with the claimed catalysis of PS in presence of Pt/Graphene electrode.

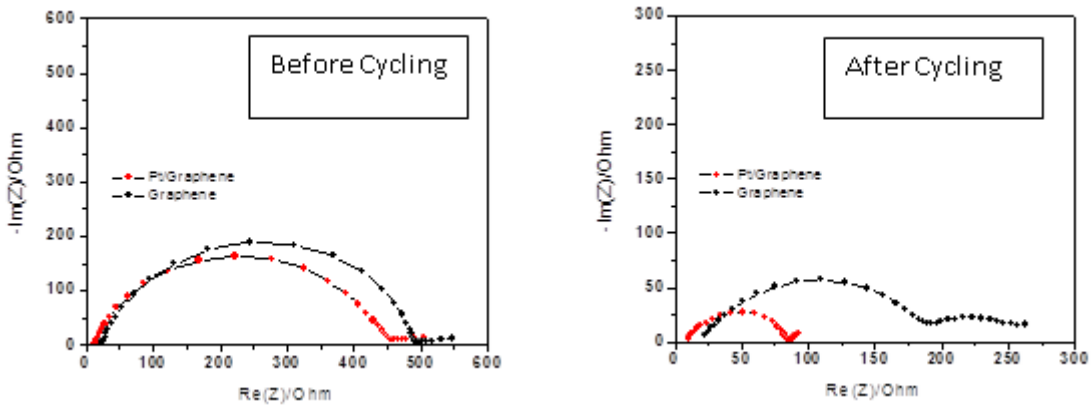

Figure 4-11 Electrochemical impedance spectra of graphene and Pt/Graphene electrodes recorded from 100 mHz to 100KHz (before and after 10 charge-discharge cycles).

In order to validate the electrocatalytic behavior of Pt/Graphene electrode towards LiPS conversions, effect of catholyte concentration and temperature on electrochemical properties has been studied. It is important to consider concentration of the starting polysulfides (catholyte), which determines the volumetric sulfur loading and hence energy density of Li-S system. The increase in the sulfur loading is expected to affect the electrochemical performance due to increase

in the viscosity of the polysulfides. However, the presence of electrocatalyst is believed to have a positive effect towards redox reactions of highly viscous catholyte.To do this feasibility study of Pt/Graphene electrode towards high sulfur loading, higher molar concentration of catholyte containing 0.8M and 1.0M Li_2S_8 (corresponds to 1.61 and 2.0 mg of sulfur per cm^{-2} respectively) have been prepared and subjected to electrochemical behaviour. Herein, Pt/Graphene electrode exhibits specific capacities of 550 and 410 mAh g^{-1} with 0.8 and 1.0 M of Li_2S_8 respectively at 0.2 C-rate with stability over 100 cycles (Figure 4-12).

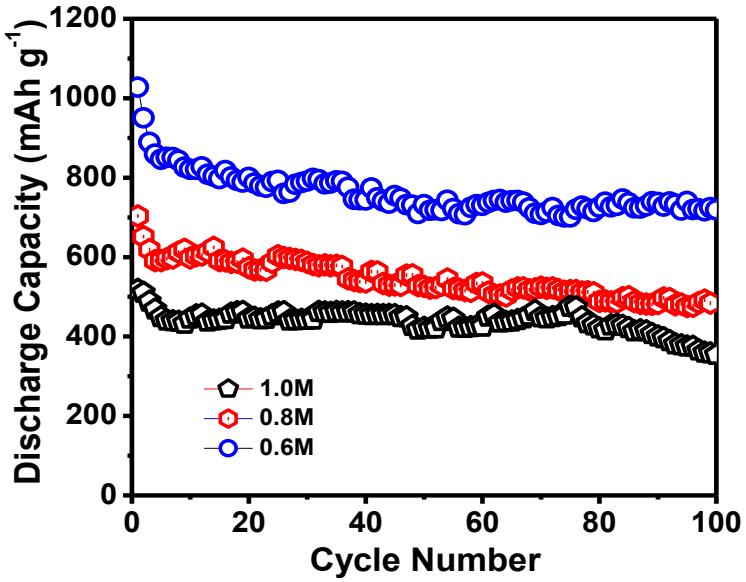

Figure 4-12 Feasibility of electrocatalyst containing electrode (Pt/Graphene) for high sulfur loading.

Pt/Graphene electrode was first cycled at room temperature for 5 cycles and then cycled at 60 °C. In agreement with electrocatalysis behavior, Pt/Graphene electrode showed significantly reduced polarization at 60 °C compared to RT with almost 50% enhanced specific capacity (Figure 4-13). Such improvements in the cell polarization and capacity with temperature confirm the electrocatalysis of polysulfides. These results including enhanced electrochemical reversibility of

LiPS highlight the significance of electrocatalytically active metal nanoparticles and their surface anchoring strength towards LiPS conversion reactions.

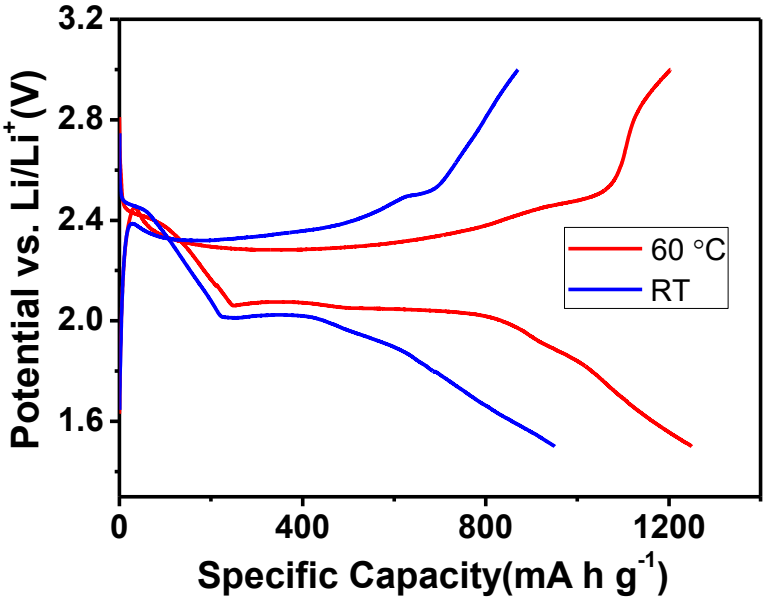

Figure 4-13 Enhancement of charge transfer kinetics (decreased charge-discharge polarization) of the Pt/Graphene electrode with increase of temperature (from 25 to 60 °C) for LiPS conversions vs Li^+/Li.

The interaction between electrocatalyst and polysulfides during charge and discharge process have been probed by conducting FESEM, XRD and X-ray photoelectron spectroscopy (XPS) studies on cycled cells. Electrodes are de-crimped carefully from 2032 coin cells, washed thoroughly with tetra ethylene glycol dimethyl ether (TEGDME) solvent and dried in vacuum for 12h. After five charge-discharge cycles, both Graphene and Pt/Graphene electrodes are examined in discharge and charged state separately. FESEM images of Graphene and Pt/Graphene electrodes at charged state are respectively shown in Figure 4-14(a,b). The presence of precipitated insoluble LiPS (some of them are marked with broken yellow lines) in Graphene electrode and its significant reduction in Pt/Graphene further evident that catalyst helps to keep the electrode structure active even after several cycles of charge/discharge process (Figure 4-15).

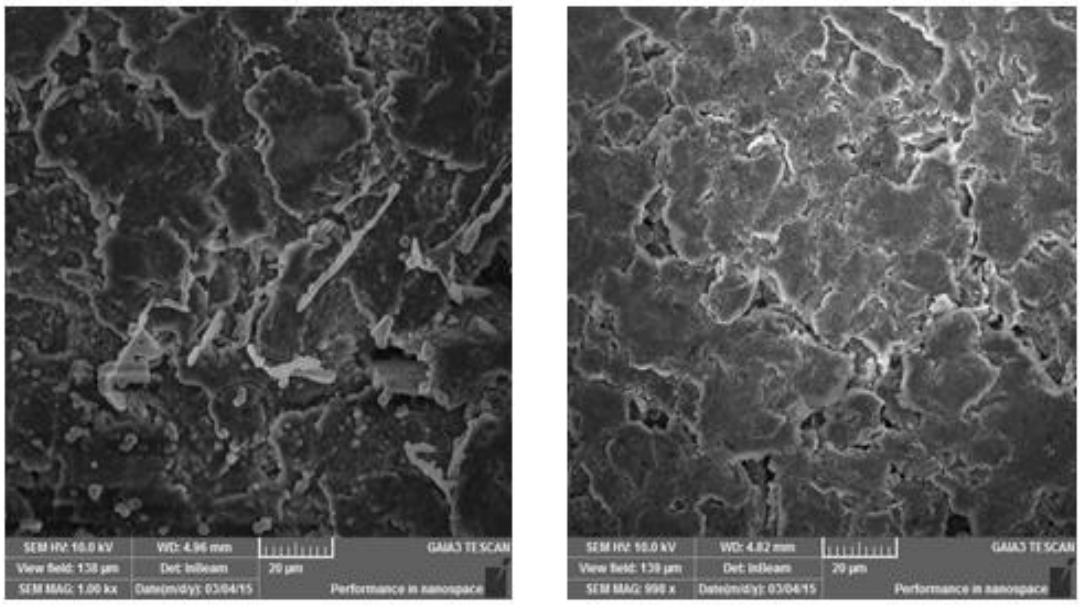

Figure 4-14 Low-magnification images of cycled electrodes a) pristine graphene and b) Pt anchored graphene at charged state.

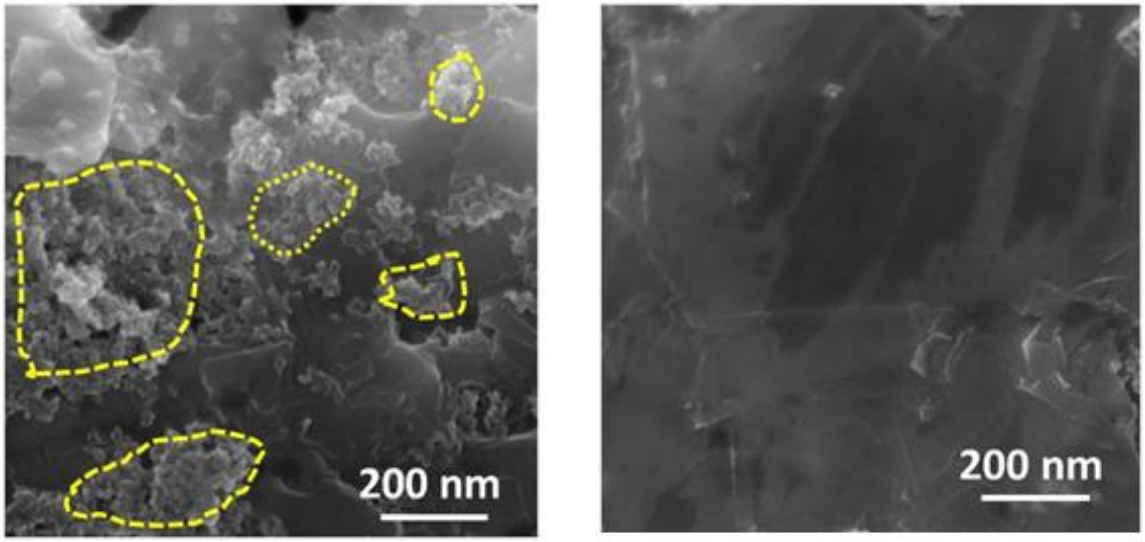

Figure 4-15 FESEM images reveal the large amount of insoluble LiPS deposition on (a) pristine graphene (highlighted in yellow circles) and (b) reduced amount of LiPS species on Pt anchored graphene

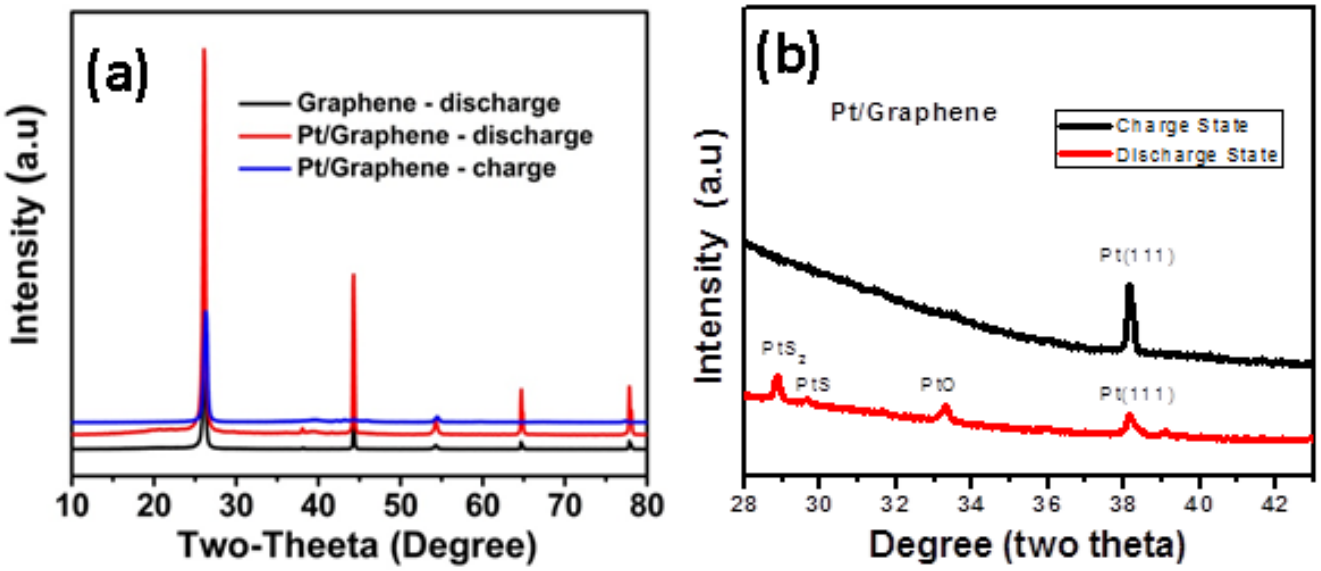

Figure 4-16 (a) XRD patterns of cycled electrodes (b) selected range of slow scan (0.5°/min.) - XRD pattern to confirm formation of Pt-S peak at discharged state and its reversibility at charged state.

From XRD patterns, formation of platinum sulfide on the discharged state (2θ=29.2° and 36.4°) and further it's fading up on charging (Figure 4-16a,b) has been observed. Hence, it is confirmed that nature of interactions between Pt and sulfur is reversible and accountable for stable electrochemical performance [92, 93].

Further, XPS spectra for Graphene and Pt/Graphene electrodes at discharged and charged state have been recorded to understand Pt-polysulfide interactions. From Figure 4-17, XPS spectra of de-convoluted S_{2p} peaks, peaks 159.3 eV corresponding to the formation of insoluble Li_2S and Li_2S_2 products observed in both discharge and charged states of Graphene electrode. The presence of such peaks in charged state indicates poor reversibility of deposited short-chain polysulfides to long-chain polysulfides. In other hand, significant reduction in the relative area of XPS peak is observed for the charged state of Pt/Graphene electrode witness the better reversibility (Table 4-

4).[86, 42, 94] The positive shift in other two peaks of Pt (charged state) at 162.7 and 163.9 eV are ascribed to S-O and S-S band, especially later evidence the formation of elemental sulfur with respect to Pt/Graphene. Furthermore, from the de-convoluted 4f $^{7/2}$ and 4f $^{5/2}$ peaks of Pt (Figure 4-18), the presence of Pt^{2+} species indicates interactions with LiPS products during discharge.[95] Decrease in presence of Pt^{2+} compared to its counterpart Pt^{0} during charge process further supports the argument that Pt aids bonding of LiPS species on electrode surface during discharge process and helps the reversible reaction during charging process. Hence, Pt nanoparticle plays crucial role in adsorbing polysulfide species during discharge process and further converting them into long-chain LiPS and elemental sulfur during charging process. As a proof of concept, the feasibility of extending this concept to non-noble metal catalyst, similar experiments have been conducted by taking bulk WC and TiC as electrodes against PS based electrolyte.

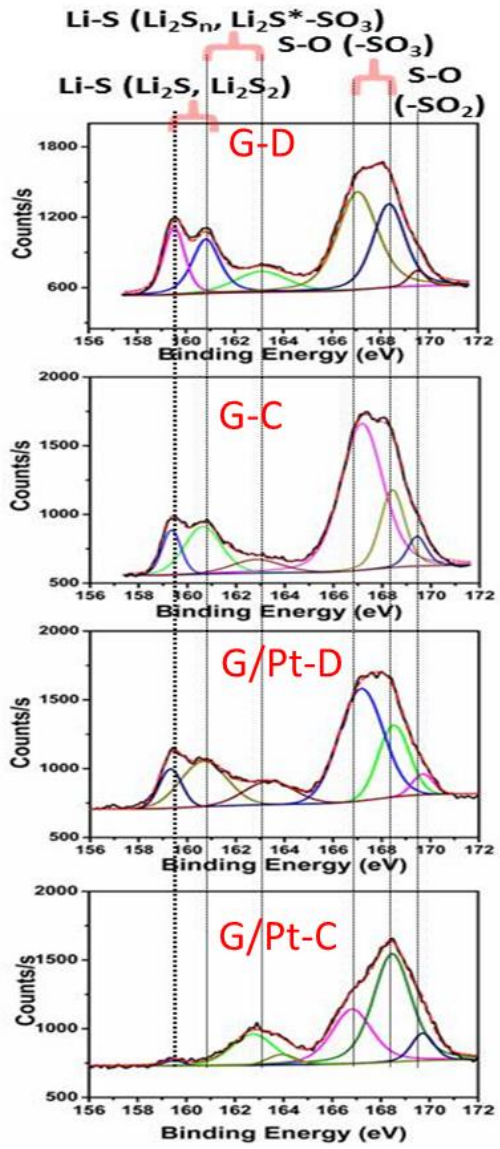

Figure 4-17 XPS analsysis (SP_2) of pristine graphene (d) & (e) and Pt/Graphene electrodes (f) & (g) in discharged and charged state respectively.

Graphene-Discharge	
Position	% Area
159.48	12.36
160.79	15.08
163.09	9.64
167.05	36.32
168.34	24.24
169.52	2.34

Graphene-Charge	
Position	% Area
159.35	6.9
160.63	14.38
162.83	5.69
167.15	51.55
168.42	17.18
169.44	4.31

Pt/Graphene-Discharge	
Position	% Area
159.31	7.55
159.31	17.88
163.37	9.91
167.15	42.11
168.49	18.86
169.69	3.7

Pt/Graphene-Charge	
Position	% Area
159.49	1.19
162.73	14.98
163.93	3.1
166.81	25.77
168.46	48.1
169.72	6.86

Table 4-4 Relative area of XPS (S_{2p}) peaks in different electrochemical conditions

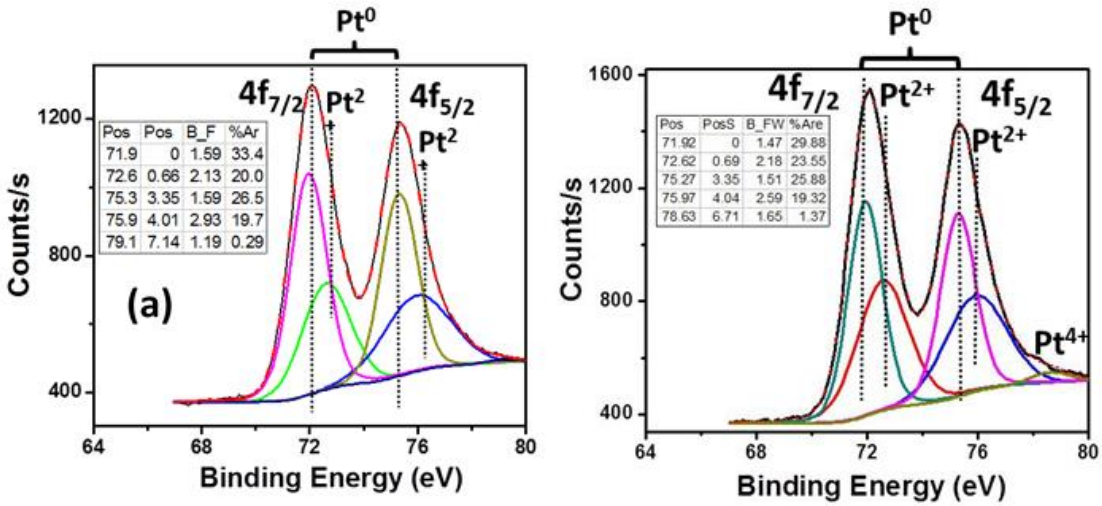

Figure 4-18 High resolution XPS scan of Pt on Pt/Graphene electrode at (a) discharged state and (b) charged state.

4.4 Conclusion:

In summary, we bring in electrocatalysis principles into Li-S battery configuration to stabilize polysulfide shuttle process and to enhance the rate capabilities. Pt/Graphene and Ni/Graphene has exhibited reduced overpotential and excellent specific capacity over pristine graphene electrodes. More importantly, presence of electrocatalyst (Pt) helps to demonstrate 40% enhancement in the specific capacity over pristine graphene with columbic efficiency above 99.3%. Postpartum analysis of electrodes further confirms the catalyst affinity towards adsorbing soluble polysulfides and converting them into long-chain polysulfides without allowing them to precipitate much on the electrode. Thus, introdusing catalyst in Li-S system will open a new avenue for improving electrochemical performance.

CHAPTER 5 SHEAR-EXFOLIATED WS_2 ELECTROCATALYSTS: CHEAP AND ALTERNATIVE FOR STABILIZING LITHIUM/SULFUR BATTERY PERFORMANCE

5.1 Introduction

In search of an efficient and cost effective electrocatalyst as an alternative to noble metals, transition-metal dichalcogenide (TMDs) materials have found attractive due their long research interest and pre-established knowledge as a catalyst in hydro-desulfurization, photocatalysis solar cells, hydrogen evolution reactions and their stability towards sulfur chemistries. Metal sulfides are considered as an alternative electrocatalysts to expensive Pt since they are relatively stable in acidic media, resistant to chemical poisoning, have exceptional mechanical robustness and more importantly possess desirable electronic conductivity [96]. Experimental and theoretical investigations of these electrocatalysts confirm that the introduction of sulfur into the lattice of the early transition metals results in an expansion of the lattice constant. Further, density functional theory (DFT) calculations have specified that the synergism among metal d-orbitals and the sulfur s^- and p^- orbitals results in broadening in the d-band structure, imparting characteristics approaching the d-band of Pt [97-99].

Among various types of TMDs available in nature, most of the literature replete with either WS_2 or MoS_2 owing to their inherent electronic and electrochemical properties, however other TMDs are progressively emerging. Due to their lamellar structure analogous to that of graphite, several well established graphene synthesis techniques such as chemical vapor deposition, wet-chemical, mechanical and electrochemical exfoliation methods have been currently adopted for the synthesis of layered TMDs. However, majority of exfoliation methods are resulted in producing small quantities of nanosheets. More importantly, applications such as energy storage and conversion devices, electrocatalyst in batteries require the substantial large amounts of 2D nanoflakes which limit their applications in various fields.

Among various methods reported to produce 2D nanosheets of TMDs, liquid-exfoliation methods has been promising due to its ability to produce bulk quantities and its precise control over flake-sizes. Recently, liquid exfoliation has been performed in aqueous solution of surfactant to produce large quantities of graphene using shear rates. A simple kitchen blender was used to exfoliate graphene sheets of equivalent quality of those produced by conventional sonication method. The significance of shear-exfoliation method over sonication technique is that achieving high volumes and higher production rates of 2D materials in a given time. Moreover, this approach utilizes water as an exfoliation medium which is eco-friendly and cost-effective especially for scaling up towards industrial applications. It is well understood that liquid exfoliation is generally produce exfoliated nanosheets with broader size and lateral dimensions. However, this could be partially addressed by optimizing or selecting post-processing steps such as altering centrifugation rates and pore size of filtration membranes. For an effective catalysis, it is reported that smaller nanosheets with length below 100nm are preferable.

With this background, large-scale synthesis and precise control over the flake size of WS_2 nanosheets has been achieved by shear-exfoliation method. The ability to tune the electrical conductivity along with high carrier mobility, layered WS_2 has become the topic of research interest in recent days especially for various opto-electronic applications. However, their catalytic properties have not thoroughly looked and their electrocatalytic properties towards polysulfide-shuttle process are utterly unknown. Herein, for the first time, we have conducted detailed investigations on electrocatalytic properties of WS_2 nanosheets to control polysulfide-shuttle process in Li-S battery. We believe electrocatalysis of polysulfides using layered TMDs will open a new avenue for developing efficient energy storage technologies.

5.2 Experimental section

5.2.1 Shear-exfoliation of WS2

In a typical experiment, bulk WS_2 (2µm, Sigma Aldrich) was dispersed in the aqueous solution of sodium cholate (Surfactant, Sigma Aldrich). The optimized ratio between bulk WS_2 and surfactant is 5:1(25:5 g) in a 500 ml millipore water for each shear-exfoliation process in a kitchen blender (Vitamix). To avoid re-stacking of exfoliated WS_2 nanosheets due to overheat of solution. The mixing has been performed for 2min with an interval rest-time of 2 min in ice-cold bath. The same cycling process was continued for 6 hours to obtain WS_2 nanosheets in surfactant solution. Firstly, well-dispersed 2D nanosheets were separated from un-exfoliated WS_2 by centrifugation at as low as 1500 rpm and followed by the concentrated supernatant liquid contains few layer WS_2 were purified and concentrated by centrifuging at 12000 rpm for 30 minutes. Finally, 2D nanosheets were collected after filtration using 0.02 µm pore size membrane using the copious amount of water to remove surfactant from exfoliated nanosheets and dried under vacuum for 12h prior to investigate their physicochemical and electrochemical properties.

5.2.2 Preparation of lithium polysulfides (Li_2S_4 and Li_2S_8)

For LiPS adsorption and electrocatalytic studies, 10 mM of lithium polysulfide (Li_2S_4) solution was used by reacting stoichiometric amount of Li_2S and S in 1:1 v/v of 1,3-dioxalane and 1,2-dimethoxyethane at 50 °C for overnight. The electro-active species containing catholyte solution (600 mM) for electrochemical properties has been prepared using calculated amounts of Li_2S and S to attain nominal formula of long-chain LiPS (Li_2S_8) in tetraethylene glycol dimethyle ether (TEGDME) at 90 °C for 12h or until all the solid particles dissolves. These molar concentrations are calculated based on the amount of active species i.e sulfur in LiPS solution.

5.2.3 Adsorption and electrocatalytic studies

Two Li_2S_4-WS_2 solutions were prepared along with blank solution (only LiPS as controlled experiment) to examine the polysulfides adsorption on WS_2 nanosheets. In a typical process, 250 and 500 µg of WS_2 were dispersed individually in 1:1 v/v of 1,3-dioxalane and 1,2-dimethoxyethane and the same was added to 1mL of LiPS (Li_2S_4) solution with an effective stirring for 30min. To speculate color changes in solution, the mixtures were undisturbed for 12h. The supernatant and WS_2 nanosheets (precipitate) were taken for ultraviolet-visible spectrophotometer (UV-Vis) and X-ray photoelectron spectroscopy (XPS) studies respectively. The electrocatalytic activity of WS_2 towards LiPS conversion reactions was performed using voltammetry techniques (CV and LSV) on three-electrode cell, consisting of WS_2 coated glassy carbon (GC) as working electrode, lithium foil as counter/reference electrodes and 10 mM Li_2S_4 solution as an electrolyte. An electrocatalyst was loaded on GC using 5 wt% nafion solution as reported previously in literature.

5.2.4 Cell fabrication and electrochemical measurements

Electrocatalytic active electrodes were prepared by an appropriate mixing of bulk WS_2 or shear-exfoliated WS_2 individually with conductive carbon (Super-P) and polyvinylidene fluoride (PVDF) binder in the weight ratio of 80: 10: 10. Such composite was taken as slurry using N-methyl-2-pyrrolidone (NMP) as solvent and coated uniformly on 18 µm thin aluminum foil. An electrode coated Al foil was dried in vacuum oven at 90 °C to evaporate NMP, and cut in to circular discs of 12.7 mm diameter. Standard 2032 coin cells were fabricated to measure electrochemical properties using coated WS_2 materials as working electrode and lithium metal as counter and reference electrode and celgard separator. Pre-calculated mount of 600 mM catholyte containing 1.56 mg of sulfur used as active material along with an electrolyte consists of 1 M of lithium

bis(trifluoromethanesulfonyl) imide (LiTFSI) and 0.1M of lithium nitrate ($LiNO_3$) in TEGDME. Linear sweep and cyclic voltammetry studies were conducted using VMP3 potentiostat (Biologic Science Instrument) in the potential window of 3.0-1.5 V at a scan rates from 0.1 mV/s. Galvanostatic charge- discharge studies were performed for WS_2 electrodes at different current rates in the potential range of 1.5 - 3.0 V using ARBIN charge-discharge cycle life tester.

5.2.5 Characterizations

X-ray diffraction (XRD) patterns are recorded at a scan rate of $0.03° s^{-1}$ on a Rigaku Miniflex II X-raydiffractometer using CuKα source. Surface morphology (Field emission electron microscopy images) studies are performed on JEOL JSM-7600 system operated with accelerating voltage 20 kV. X-ray photoelectron spectrums (XPS) of electrode surfaces have been collected using PHI Quantera spectrophotometer. Transmission electron microscopy (TEM) images were recorded on JEOL 2010 TEM using LaB6 Filament Gun. Raman studies have been carried out on Triax 550 (Horiba Jobin Yvon, Edison, NJ) with a 514 nm laser excitation.

5.3 Results and discussion

Liquid exfoliation is considered as one of the favorable way to produce large-scale nanosheets of TMDs to meet their potential applications. In a typical experiment, shear-exfoliation process is performed to exfoliate tungsten sulfide (WS_2) using simple kitchen blender in aqueous surfactant solution. Sodium cholate has been used as surfactant to stabilize exfoliated nanosheets, however, the ratio of WS_2 and surfactant (sodium cholate) at start of the experiment is predominantly determines the quality of nanosheets. The shear-exfoliated WS_2 nanosheets were washed thoroughly to remove surfactants and vacuum dried for overnight, subsequently subjected for their physical and electrochemical studies. As shear-exfoliated WS_2 along with bulk

counterpart are characterized systematically using microscopy, X-ray diffraction (XRD), X-ray photoelectron (XPS) and Raman spectroscopy techniques.

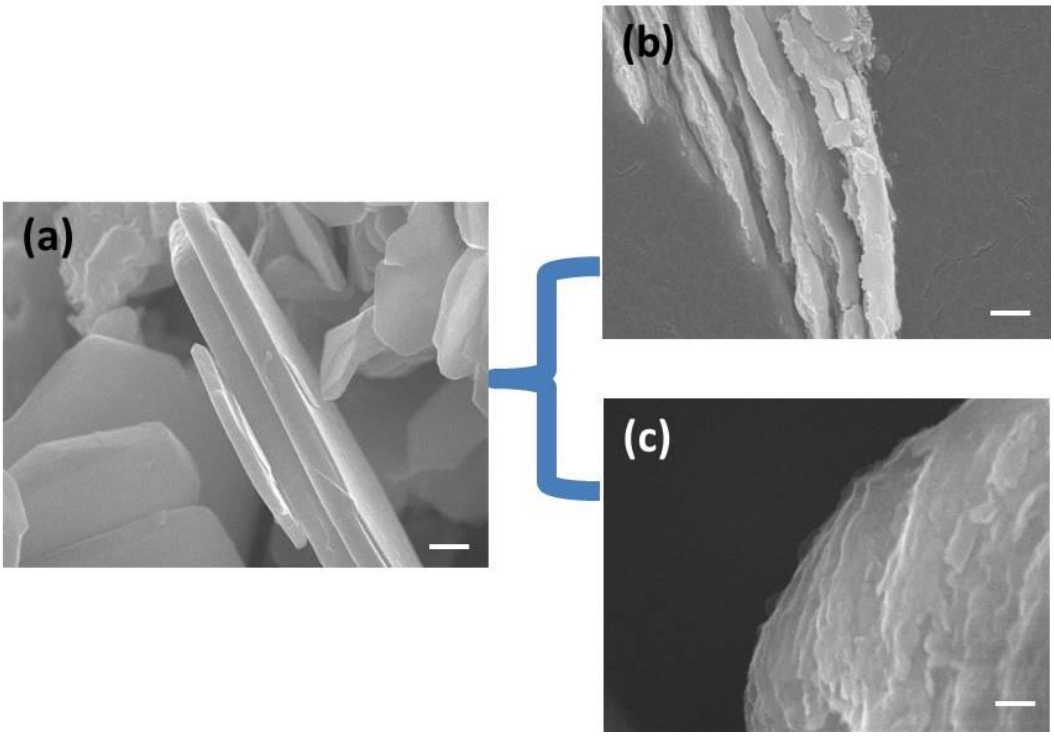

Figure 5-1 FESEM images of (a) bulk WS_2, (b) and (c) WS_2 nanosheets produced via. Shear-exfoliation process in surfactant containing aqueous solution (Scale bars represent 1 µm)

Field emission scanning electron microscopy (FESEM) image of bulk WS_2 was shown large polygonal stacks up to hundreds of nanometer thicknesses with the few micrometer flake sizes (Figure 5-1). Upon shear-exfoliation, a significant disintegration of WS_2 flakes across its width represents a successful exfoliation in aqueous solution. Such exfoliated flakes have been observed along with extensive wrinkling of the edges, as expected from shear force generated by high shear rate during the blending process.

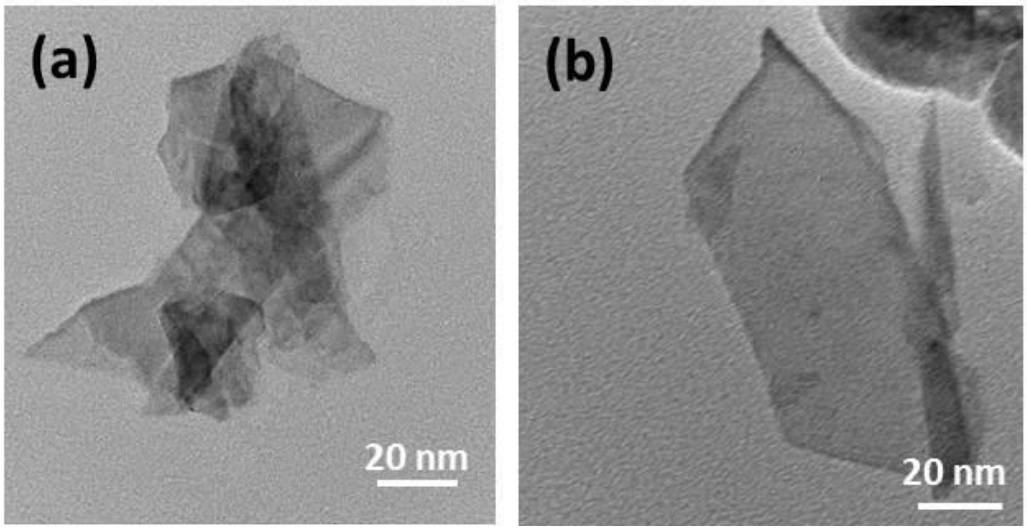

Figure 5-2 TEM images of WS_2 nanosheets produced via. shear-exfoliation process.

To further observe nature of dispersed nanosheets resulted from shear-exfoliation of WS2, transmission electron microscopy (TEM) study has been performed. Figure 5-2a and b have shown the TEM images of shear-exfoliated WS_2 nanosheets with a narrow distribution of nanosheets with desirable lateral dimensions. Unlike, other liquid exfoliation methods, which yield broad range of flake sizes, shear exfoliation resulted in planar objects with the small lateral size below 100 nm which is suitable for electrocatalysis. Herein, images were proven the successful exfoliation of nanosheets with folded edges.

In addition, we have investigated X-ray diffraction (XRD) patterns (Figure 5-3a) and Raman spectrums (Figure 5-3b) for exfoliated WS_2 in comparison with its bulk to evaluate further exfoliated WS_2 nanosheets. In XRD study, both the samples exhibit identical patterns with significant reduction in peaks intensity, especially for (002) reflection at $2\theta=14.24°$ which is another indication for production of WS_2 nanosheets via. shear-exfoliation process [100]. Similarly, raman spectra of both bulk and exfoliated WS_2 display two strong peaks at 350 and 415 cm^{-1}. However, the intensity ratios of Raman peaks reveal the distinguishable evidence that the

quality of shear-exfoliated WS_2 nanosheets. Yet another information gained from Raman spectroscopy is that no vibration due to impurities (for example, no surfactant are detected).

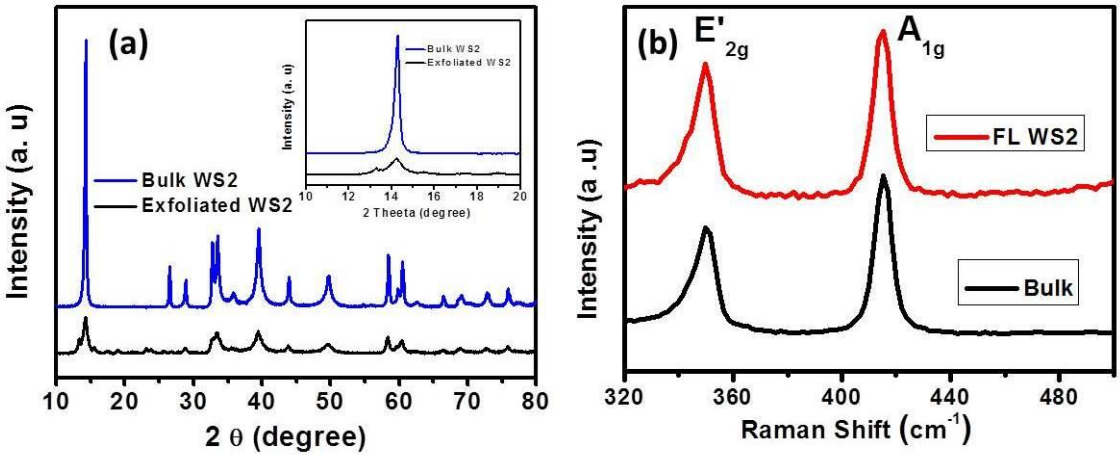

Figure 5-3 XRD patterns of (a) bulk WS_2 and shear-exfoliated WS_2 nanosheets (Inset: selected area to highlight (002) reflection) and (b) Raman spectra of shear-exfoliated WS_2 nanosheets in-comparison with its counterpart bulk WS_2

In spite of insights gained from microscopy, XRD and Raman studies, chemical and structural transformation on surface about shear-exfoliated WS_2 was insufficient, especially towards electrocatalytic phases. It is well-documented that 1T phase of TMDs are greatly influenced their electrocatalytic activity towards any red-ox reactions. In this regard, X-ray photoelectron spectroscopy (XPS) measurements were performed on both the materials to examine elemental composition and phase analysis upon exfoliation. Figure 5-4a and b illustrates the XPS spectra of W 4f orbitals for both the samples, observed peaks at 34.3 and 32.2 eV are correlated to W^{4+} $4f_{5/2}$ and $4f_{7/2}$, respectively. At this juncture, we have also determine a peak at 37.9 eV on both the spectra corresponding to oxidized W(IV), as reported previously [101]. Upon deconvoluted the W4f, three distinguishable peaks have been observed for both the samples mostly due to 2H phase, 1T phase and oxidized W(IV). However, their difference in atomic percentages corresponding to different phases reflects the relative structural changes on surface resulting from

exfoliation as tabulated in Figure 5-4c. Even though, XPS alone is not an appropriate technique to analyze elemental composition of 2-D materials, it is important to note that comparison of their ratios holds good and generally gives close approximations. It is well reported that 1T phase is metallic in nature and high in electrocatalytic activity towards any red-ox reaction. Hence, exfoliated WS_2 nanosheets with enhanced 1T phase is expected to exhibit better electrode with LiPS conversions.

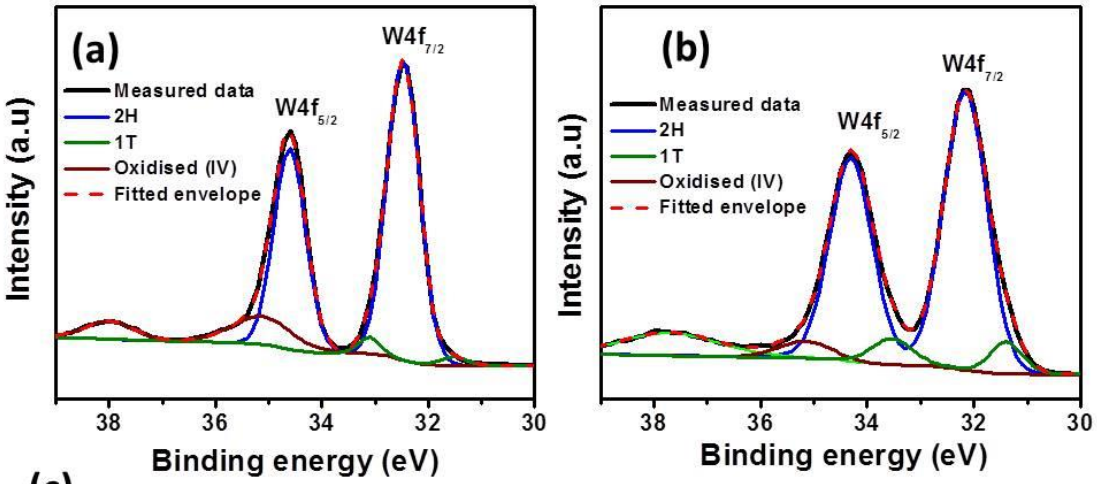

(c)

Material	Surface Sulfur/Tungsten Ratio	1T(at.%)	2H(at.%)	W(IV)(at.%)
Bulk WS_2	1.6	3.11	83.47	13.42
Exf. WS_2	2.06	8.29	79.4	12.31

Figure 5-4 X-ray photoelectron spectra of shear-exfoliated WS_2 and its counterpart bulk WS_2 (a) W4f of bulk, (b) W4f of exfoliated WS_2-nanosheets and (c) tabulated atomic percentage of different phases respectively

To understand the adsorption of lithium polysulfides (LiPS) on layered TMDs which advances reversible red-ox reactions, we have prepared medium chain-length Li_2S_4 as represented LiPS and verified their adsorption behavior with WS_2 using ultraviolet-visible spectrophotometer (UV-Vis). The known amount of WS_2 material is added to the 1ml of 0.01 M Li_2S_4 solution

prepared in a mixture of 1,3-dioxolane and 1,2-dimethoxyethane(1:1V/V), stirred for 30 minutes and kept for overnight as undisturbed.

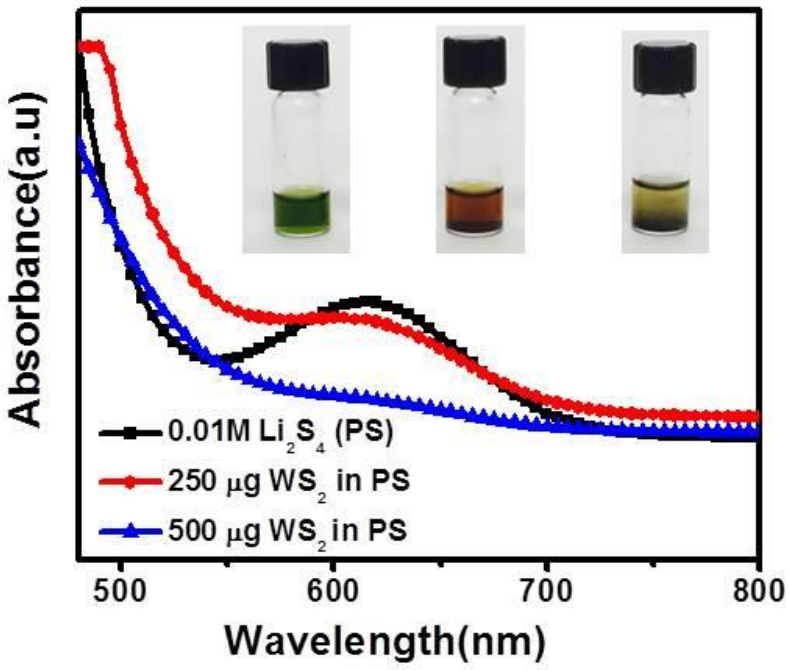

Figure 5-5 UV absorption studies of lithium polysulfides and corresponding visual inspection of LiPS color changes upon their adsorption on WS_2 nanosheets (inset)

On visual inspection, green solution turned to light-reddish green with 0.25mg of WS_2 indicating part of ionic species getting adsorbed on solid matrix. With the increase of the WS_2 concentration, a complete change in LiPS color has been observed as shown in Figure 5-5 (inset). Further, the same interactions have been confirmed analytically from UV absorption study wherein a strong absorption peak is identified at 600 nm correlated to the dissolved lithium polysulfides. The absorption peak is completely diminished upon addition of WS_2 confirms the LiPS affinity towards layered TMDs.

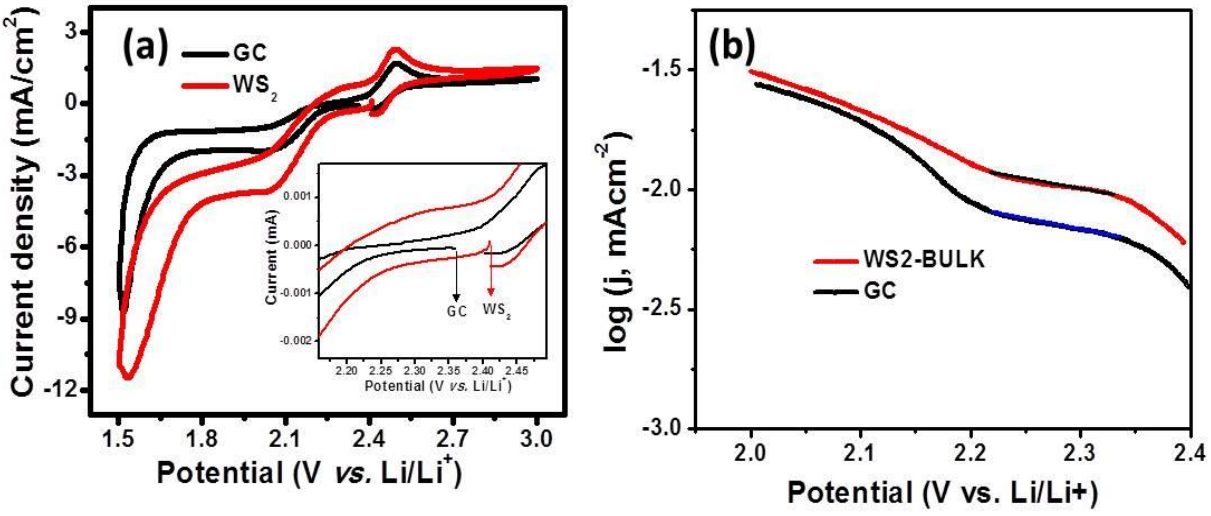

Figure 5-6 (a) Representative cyclic voltammograms of WS_2 nanosheets and bulk WS_2 vs. Li/Li+ with Li_2S_4 solution as an electrolyte and (b) Tafel plot derived from linear sweep voltammetry

Cyclic voltammetry (CV) and Linear sweep voltammetry (LSV) studies were conducted to understand the kinetics of WS_2 nanosheets towards LiPS red-ox reactions using standard three-electrode cell in 10mM of Li_2S_4 solution containing 1M LiTFSI salt as electrolyte. The electrocatalyst was loaded on a glassy carbon electrode and used as a working electrode vs. metallic lithium as reference and counter electrodes. Figure 5-6a displays the representative CV performance of WS_2 and its comparison with commercial carbon electrode at a scan rate of 0.1mV/s. Considerable changes in the LiPS red-ox reactions were observed in terms of current density and onset potentials of red-ox peaks. The derived parameters from CV's such as onset potentials (Epa, Epc) and peak current densities (Ipa/Ipc) along with exchange current density values (derived from LSV) are tabulated in Table 5-1. The positive shift of onset potentials for the reduction of LiPS are 2.24 and 1.78 V (for carbon, 2.21 and 1.67 V) and negative shift in oxidation of LiPS is 2.39 V (for carbon, 2.42 V) respectively have been observed for WS_2 nanosheets compared to carbon electrode.

In addition, LiPS red-ox peak current densities of WS_2 electrode is much higher than that of carbon electrode, demonstrating the electrocatalytic effect of WS_2 nanosheets electrode. Such an enhanced behavior is mainly attributed to available edge and basal planes (1T-phase) resulted in shear-exfoliation of WS_2 as confirmed by XPS. Comparatively, improved non-Faradaic current for WS_2 electrode is an indication of high surface area. The kinetic parameters are derived by conducting LSV experiments on both the electrodes. During LSV technique, we sweep-down from OCV to 400 mV for cathodic process at a scan rate of 0.1mV/s. Similarly, oxidation sweep has been carried out after electrodes discharged completely (up to 1.5 V) and rested for couple of hours to attain the equilibrium state. The exchange current density values have been obtained from Tafel plot drawn using potential vs. current values Figure 5-6b. Hence, superior electrocatalytic activity and reversibility of LiPS reactions for WS_2 nanosheets are evident that it could exhibit better electrochemical performance.

Electrode	OCV (V)	Onset potentials (V)		Peak currents (mA)		Exchange current density
		Reduction	oxidation	Reduction	Oxidation	
Carbon	2.36	2.21, 1.67	2.42	8.5	1.71	2.52
WS_2	2.41	2.24, 1.78	2.39	11.5	2.35	8.53

Table 5-1 Derived electrochemical parameters from CV and LSV

Electrochemical performance of 2-D WS_2 nanosheets and its bulk counterpart has been evaluated by fabricating standard 2032 coin cells. The cells consisting of titled compounds as working electrodes vs. metallic lithium foil as counter/reference electrode and celgard membrane as a separator. Herein, the electrochemical active species are in the form of LiPS (0.6M of Li_2S_8) in TEGDME solution containing 1M of lithium bis(trifluoromethanesulfonyl) imide (LiTFSI) and 0.1M lithium nitrate (LiNO3). Electrochemical properties were measured at a constant current rate

of 0.2 C (The full discharge-charge capacity of 1672 mAh/g in 5 h) in a potential window between 3.0-1.5 V. Figure 5-7 displays galvanostatic discharge-charge profiles and cycling performance of bulk WS_2. A well-defined voltage vs. capacity plateaus corresponding to LiPS red-ox reactions upon number of cycles are strong indication of electrode/electrocatalyst behavior for newly identified WS_2 (Figure 5-7a). Typical two-discharge plateaus related to the conversion of long-chain LiPS to medium (Li_2Sx, $6 \leq x \geq 8$) at 2.4 V and then followed by further conversion to short-chain LiPS at 2.0 V. For an initial few cycles of discharge, there is a lower-voltage plateau around 1.7 V is attributed to formation of insoluble product Li_2S, thus responsible large capacity fade at first few cycles. Even with after several cycles, the voltage vs. capacity plateaus have been observed overlap each other at 2.4 and 2.0 V, which is an indication of the suitability of newly identified electrocatalytically active TMDs i.e WS_2 electrode for longs cycling of Li-S battery

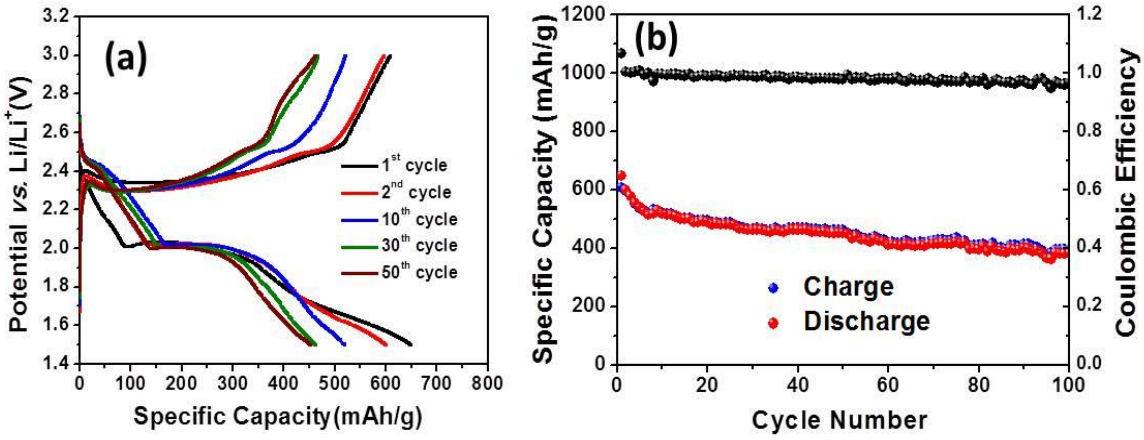

Figure 5-7 (a) Charge-discharge profiles and (b) cycle life performance of bulk WS_2 in the potential range 1.5-3.0V

Figure 5-7b demonstrations the cycling behaviour of WS_2 cathode for 100 cycles at 0.2 C rate with coulombic efficiency of ~98.5%. Apart from few initial cycles, for instance, from 10 to 100 cycles capacity fade is almost negligible due to an effective improved reversibility of LiPS on

WS_2 surface. At the end of 100th cycle, the cathode consists of bulk WS_2 electrode delivers the capacity of 416 mAh/g.

An electrode was found to show enhanced performance with plateaus of charge-discharge around 2.4 and 2.0 V respectively with reduced polarization and it has been observed to be consistent over the long cycles (Figure 5-8a). Though, bulk WS_2 exhibit reasonable capacity over a one hundred cycles, another key point that poor coulombic efficiency upon number of cycles limits its use as electrode for Li-S battery (Figure 5-8b). Furthermore, owing to large surface area and more number of available active sites for LiPS red-ox reactions, shear-exfoliated WS_2 enhances not only charge-discharge efficiency but also electrochemical properties. Hence, WS_2 demonstrates as an efficient electrocatalytically active electrode towards LiPS conversion reactions with high specific capacity of 630 mAh/g (Figure 5-8b).

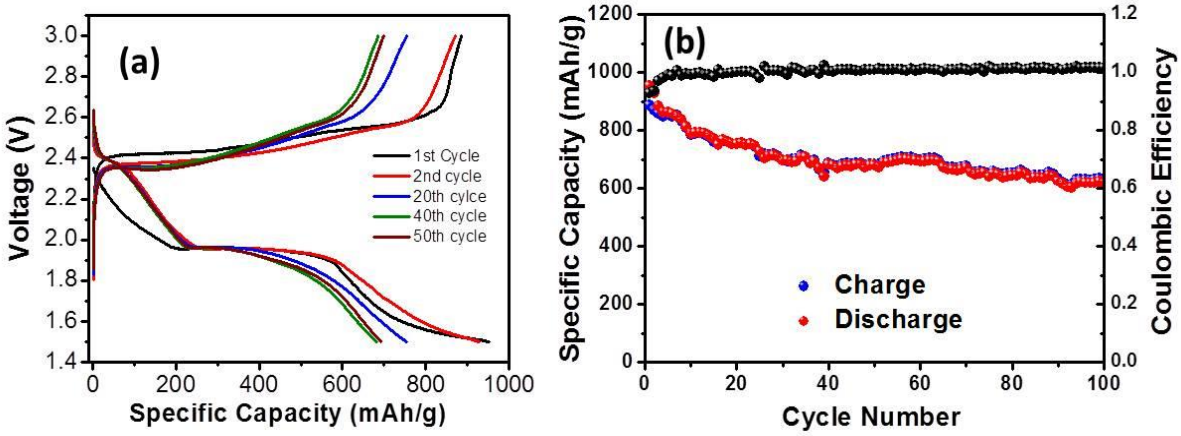

Figure 5-8 (a) Galvanostatic charge-discharge profiles and (b) cycle life performance of shear-exfoliated WS_2 nanosheets as electrode in the potential range 1.5-3.0V

The shear-exfoliated WS_2 nanosheets have been examined further for high rate capability and obtained results depicted in figure 5-9. As expected, the electrode consist of WS_2 nanosheets exhibited an excellent high power rate capability as its exhibits as high as 380 mAh/g at 1 C rate. Also, the retention in the capacity and columbic efficiency at high rate charge-discharge rate at 1C

for more than 250 charge-discharge cycles could be understood from the figure. Thus we could understand from detailed electrochemical and electrocatalytical studies, shear-exfoliated WS_2 nanosheets are effective to control LiPS shuttle mechanism to stabilize Li-S battery performance.

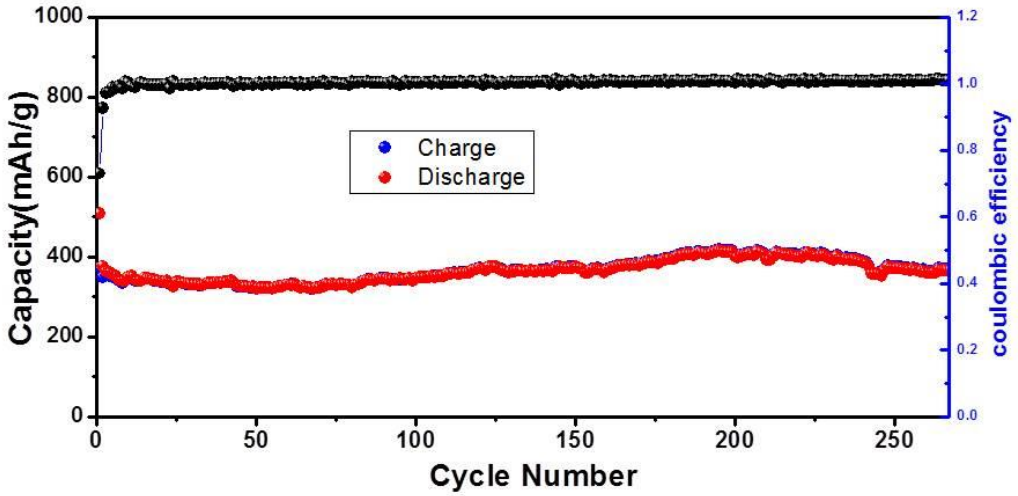

Figure 5-9 Long cycling behavior of WS_2 electrode at 1C rate

5.4 Conclusion

Controlling polysulfide-shuttle process in rechargeable Li-S battery holds key for realizing its potential applications. Herein, we demonstrated successfully electrocatalysis approach to control polysulfide-shuttle process using shear-exfoliated WS_2 nanosheets. Large-scale production and precise control over the flake size of WS_2 nanosheets has been achieved using shear-exfoliation method. Electrocatalytic activity of WS_2 nanosheets towards LiPS conversion reactions during charge-discharge process has been studied thoroughly. Electrochemical properties of WS_2 nanosheets have been investigated by systematically varying catalytic active sites, rate-capabilities of the Li-S cell. Unveiling a specific capacity of 630 mAh/g at 0.2C rate and 380 mAh/g at 1C rate with excellent stability over 300 cycles clearly indicates yet another promising application of 2D layered metal chalcogenides.

CHAPTER 6 METAL CARBIDE NANOPARTICLES AS EFFICIENT ELECTROCATALYSTS FOR LITHIUM POLYSULFIDE CONVERSION REACTIONS

6.1 Introduction

Numerous scientific and engineering approaches also have been implemented and directed research to develop cathodes to improve the performances. In our previous chapter, we followed a different approach and demonstrated the utilization of nanostructured Pt and Ni electrocatalytic materials to trap polysulfides thereby improving the Li-S battery performances. In the present work, we have investigated the feasibility/applicability of using a new class of cathodes, specifically transition metal carbides, in Li/dissolved polysulfide battery configuration. Transition metal carbides have been used as catalyst for many electrochemical reactions including hydrogen evolution, oxygen reduction, H_2O_2 reduction, methanol oxidation and ethanol oxidation and also industrially important desulfurization, isomerization and hydrogenolysis processes due to their unique physicochemical properties and Pt-like behavior [106]. The electrochemical activities of transition metal carbides are thought to relate to the 3d electron number of transition metal atoms and strong interactions between metal and electroactive species. We anticipate the characteristics of transition metal carbides such as high metallic conductivity, high work function, chemisorption of sulfur species via metal–sulfur interactions, redox ability, and excellent thermal/mechanical stability will help in improving the polysulfide conversion kinetics as well as battery cycling performances. Nanostructured tungsten carbide (WC) and titanium carbide (TiC) powders were synthesized and characterized [107, 108]. Electrochemical studies along with ex-situ microscopic/spectroscopic studies were carried out to investigate discharge/charge processes and physical insights about the interactions between metal carbide and polysulfides were provided in detail.

6.2 Experimental preparation

6.2.1 Preparation of tungsten carbide (WC)

In a typical synthesis, 6.5 g ammonium paratungstate $(NH_4)_6W_7O_{24}$ was dissolved in 300 ml of de-ionized water and followed by adding 1.8 g activated carbon (Vulcan XC-72R, Cabot corporation). This mixture was stirred vigorously at 343 K for 2 h to realize complete wetting of carbon and impregnation of tungsten ions. Then the solvent was fast evaporated at 373 K under continuous stirring. The resulting solid was further dried at 343 K for 6 h in a vacuum oven and then calcinated at 723 K for 2 h. In succession, this solid was carbonized at 1223 K with a heating rate of 5 K/min under a CO stream (flow rate: 180 to 200 ml/min) and maintained at 1223 K for 8 h. After slow cooling to room temperature, the final product was obtained.

6.2.2 Preparation of titanium carbide (TiC)

In a typical synthesis, 1.6 titanium dioxide, 2.43 g magnesium carbonate and 2.92 metallic magnesium powders were mixed thoroughly and loaded into a 50 mL capacity stainless steel autoclave. All the manipulations were carried out in a dry glove box. After sealing under inert gas atmosphere, the autoclave was heated from room temperature to 823 K at a heating rate of 10 K/min, and maintained at 823 K for 10 h, followed by cooling gradually to room temperature in the furnace. The product obtained from autoclave was washed several times with dilute HCl and distilled water to remove the impurities. Finally, the product was washed with absolute ethanol and vacuum-dried at 333 K for 12 h.

6.3 Results and discussion

6.3.1 Diffraction and microscopic analyses of the transition metal carbides

Structural features of the prepared metal carbides were analyzed using powder XRD. Diffraction patterns of WC and TiC are indexed and presented in Figure 6-1a and d, respectively. Analysis of the Bragg peaks representing hexagonal WC phase with space group, $P6_3mc$ (No. 186) and cubic TiC phase with space group, *Fd3c* (No. 225). Broad diffraction peaks are indicative of nanocrystalline nature. No peaks corresponding to the metal oxides or amorphous carbon were noticed, indicating phase purity of the materials. Morphological features of the metal carbides were examined using FESEM and TEM. SEM images depicted the agglomeration of crystallites in the size range of 80-120 nm for WC (Figure 6-1b) and 20-25 nm for TiC (Figure 6-1e). Close examination of the particles by TEM depicted three-dimensional network of interconnected crystallites without any impurities (Figure 6-1c and f). It ensures the electronic conductivity.

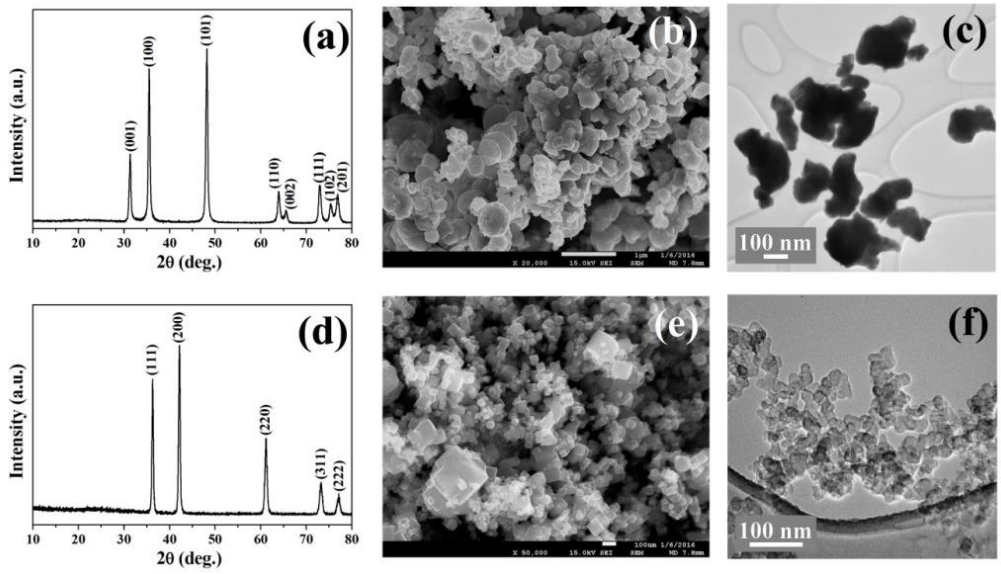

Figure 6-1(a,d) XRD, (b,e) SEM, and (c,f) TEM of WC and TiC. First and second rows correspond to the WC and TiC, respectively.

Further, purity of the materials was further confirmed by composition analysis using EDX. EDX spectral and element mapping analysis indicated the presence respective elements and also the elemental distributions for all metal carbide samples are close to their original ratios (Figure 6-2).

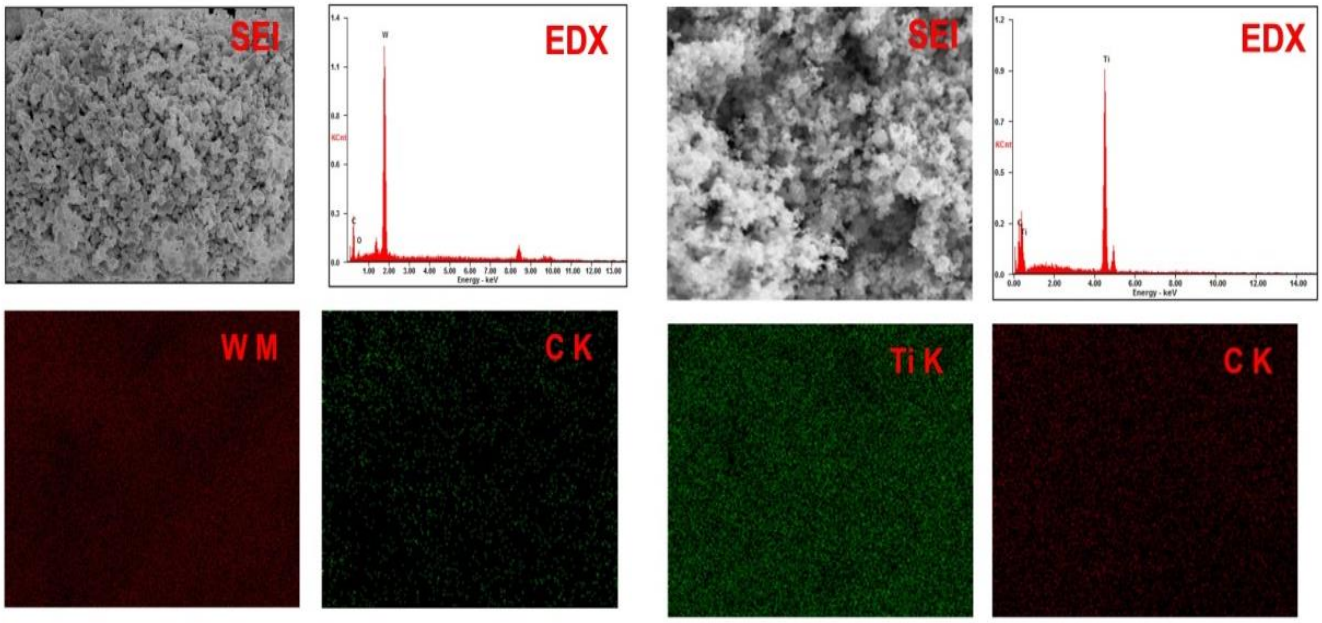

Figure 6-2 Secondary electron image (SEI) with corresponding EDX spectrum and elemental mapping images of WC and TiC

6.3.2 Electrochemical properties

To evaluate the electrochemical performance of metal carbides such as WC and TiC, standard 2032 coin cells were fabricated using them as cathode *vs* metallic lithium as an anode and dissolved Li_2S_8 in electrolyte (0.6 M and 10 µl) as an active material. Figure 6-3 illustrate that representative CV of WC and TiC electrodes vs. Li/Li^+ at a scan rate of 0.1 mV/s with 10 µl of Li_2S_8 in TEGDME solvent containing 1M LiTFSI and 0.1M $LiNO_3$ as catholyte. Recorded CV curves for both the carbides consist of two cathodic peaks at 2.44 and 1.9 V corresponding to transformation of long-chain lithium polysulfides to short-chain LiPS and

subsequent reduction to lower lithium polysulfides respectively. Upon forward scan, anodic peak has been observed related to reversible conversion of short-chain to long-chain LiPS which results in excellent reversibility[88]. Further, as a comparison between WC and TiC, the high red-ox peak currents for TiC indicating that stability or better activity of electrocatalyst. Similarly, onset potentials for TiC have been observed are 1.91 and 2.38 V resulting in reduced polarization to that of WC attributed to narroowly distributed TiC nanoparticles as understood from SEM images.

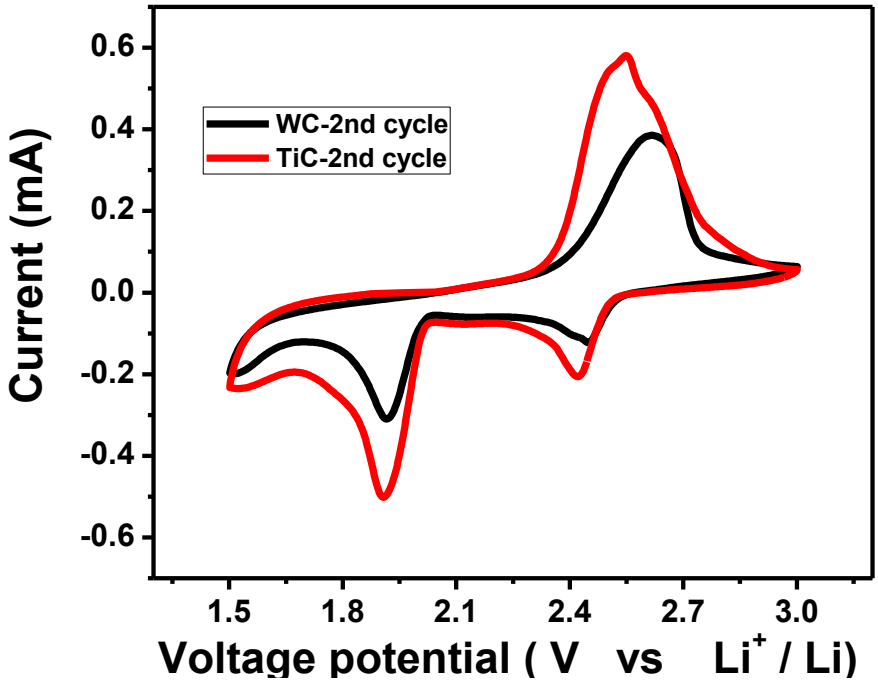

Figure 6-3 Cyclic voltammetry for both TiC and WC at scan rate of 0.1mV/s between the potential range of 1.5-3.0V

Electrochemical behaviour of metal carbides was studied at a constant current rate of 0.1 C (based on sulfur mass in the cell) and obtained results have been displayed in Figure 4 and 5. Initial charge-discharge capacities of 720 mAh/g at a c-rate of 0.1C with stability over 530 mAh/g are realized over 185 cycles (from figure 6-4a), which reveals robustness of WC electrode even after long cycling. Figure 6-4b depicts the charge-discharge profiles of the cell containing WC

electrocatalyst. A stable voltage plateaus with comparable polarization between charge-discharge plateaus have been observed.

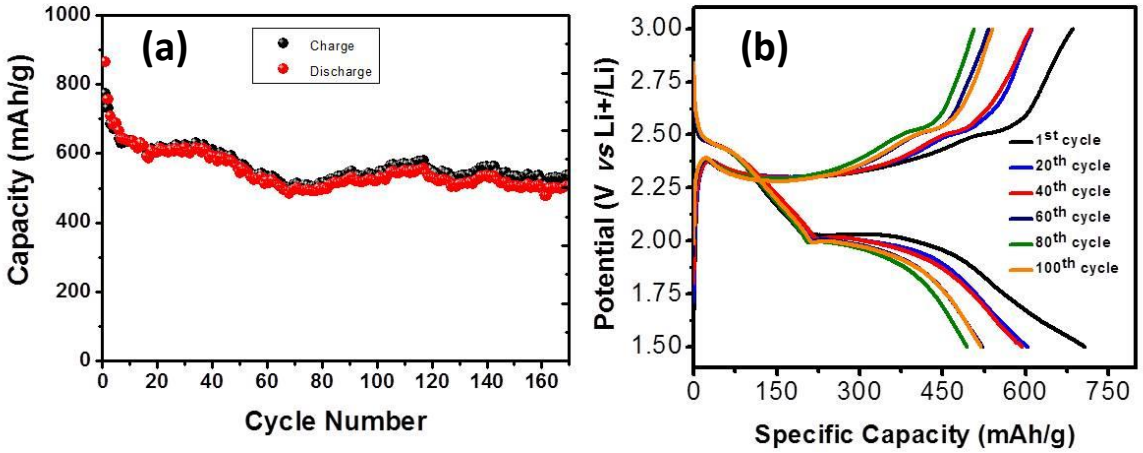

Figure 6-4 Galvanostatic cycling behavior and charge-discharge profiles of WC electrocatalyst with 0.6M Li_2S_8 catholyte in the potential window of 1.5 - 3.0 V

Similarly, galvanostatic measurements are conducted on TiC as cathode vs. Li/Li^+ at a constant current rate of 0.1 C (based on sulfur mass in the cell) and obtained results have been monitored for 100 cycles. Figure 6-5a shows that type of electrocatalyst plays a crucial role in polysulfide conversion process, thus related electrochemical properties. Herein, TiC exhibit as high as specific capacity 1300 mAh/g, however, it has been observed that capacity fade occurs for first few cycles. Figure 6-5b reveals that TiC nanoelectrocatalyst electrode exhibited well defined typical discharge plateaus corresponding to the formation of soluble long-chain PS and their spontaneous dissociation to short-chain PS at plateaus at 2.4 and 1.97 V and reversible conversion of short-chain to long-chain LiPS plateaus at 2.34 V during charging process.

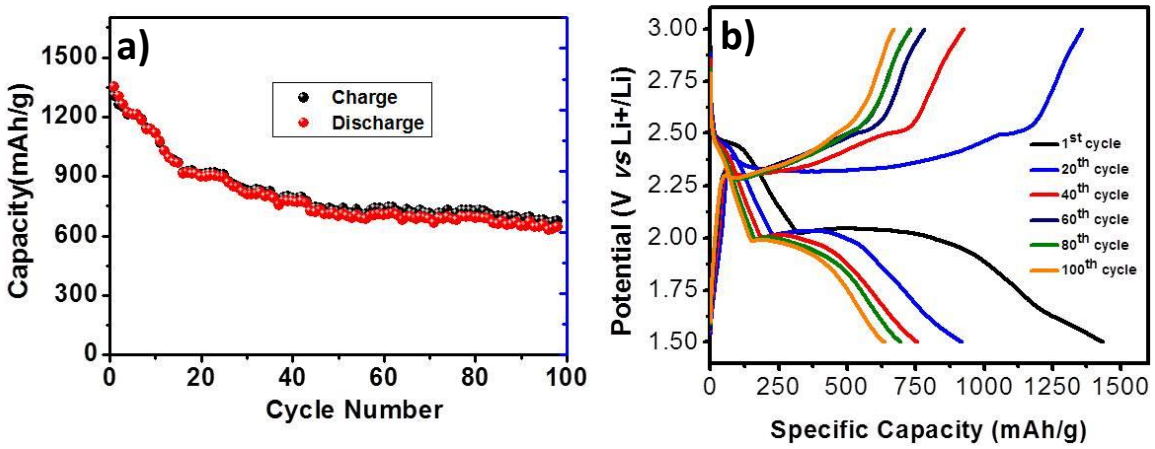

Figure 6-5 Cycling behavior and charge-discharge profiles of TiC electrocatalyst with 0.6M Li2S8 catholyte in the potential window of 1.5 - 3.0 V

6.4 Conclusions

Owing to high electrical conductivity, PS adsorptivity due to polared nature and high work function, metal carbides are promising as one of the efficient electrocatlyst/electrodes for advanced Li-S batteries. Herein, metal carbides such as WC and TiC are synthesized successfully via. carbothermal reduction process with desired particle size of about 100 nm. Electrochemical properties of these MCs towards LiPS conversion reactions are examined by conducting galvanostatic charge-discharge studies. Among studied MCs, TiC exhibited specific capacity of as high 1300mAh/g for initial cycles, however, detailed analysis with respect to their electrocatalytic activity. The rate performance capability and long cycle life are under study.

CHAPTER 7 CONCLUSIONS AND FUTURE WORKS

In summary, we bring in electrocatalysis principles into Li-S battery configuration to stabilize polysulfide shuttle process and to enhance the rate capabilities. As a proof of concept, we have studied LiPS conversion reactions with Pt/Graphene and Ni/Graphene vs. Li/Li+ in sulfur containing catholyte solution. Such an electrocatalytically active electrodes, especially Pt/graphene composite has exhibited reduced overpotential and excellent specific capacity over pristine graphene electrodes. More importantly, presence of electrocatalyst (Pt) helps to demonstrate 40% enhancement in the specific capacity over pristine graphene with a coulombic efficiency above 99.3%.

In search of an efficient and cost effective electrocatalyst as an alternative to noble metals, transition-metal dichalcogenide (TMDs) and metal carbides (MCs) have found attractive due their long research interest and pre-established knowledge as a catalyst in hydro-desulfurization, photocatalysis solar cells and hydrogen evolution reactions and their stability towards sulfur chemistries. They have specified that the synergism among metal d-orbitals and the sulfur or carbon s^- and p^- orbitals results in a broadening in the d-band structure, imparting characteristics approaching the d-band of Pt. Electrocatalytic activity of WS_2 nanosheets towards LiPS conversion reactions during charge-discharge process has been studied thoroughly. Electrochemical properties of WS_2 nanosheets and MCs have been investigated by systematically varying catalytic active sites, rate-capabilities of the Li-S cell. Unveiling a specific capacity of 630 mAh/g at 0.2C rate and 380 mAh/g at 1C rate with excellent stability over 300 cycles clearly indicates that newly identified materials are promising electrodes for Li-S battery applications. The nature of interactions between electrodes and LiPS species further confirms the catalyst affinity towards adsorbing soluble polysulfides and converting them into long-chain polysulfides without allowing them to

precipitate much on the electrode. Thus, introducing catalyst in Li-S system will open a new avenue for improving electrochemical performance.

Conversion of lower polysulfides to higher polysulfides and trapping them in a conductive highly porous matrix especially carbon based materials with wide variety of shapes and size or at cathode has been considered as crucial step in the sulfur based battery technologies. It is well know that the energy and power density of sulfur based battery configurations including Metal/sulfur, Metal/polysulfide and Redox flow batteries depend on rate of polysulfides conversion process. With this background, we recommend following materials and strategies for future works

- Identification and synthesis of large surface area and porous electrocatalysts to trap dissolved lithium polysulfides and convert them effectively during charge-discharge process. For examples, Metal nitrides, metal containing zeolites.
- The same electrocatalysis approach could be applied to other metal polysulfides battery chemistry to improve reaction kinetics and hence overall energy density and power density of the battery system improves. For example, Na-S, Mg-S battery systems

REFERENCES

1. Tarascon, J.-M. and M. Armand, *Issues and challenges facing rechargeable lithium batteries.* Nature, 2001. **414**(6861): p. 359-367.
2. Nitta, N., et al., *Li-ion battery materials: present and future.* Materials Today, 2015. **18**(5): p. 252-264.
3. Kang, B. and G. Ceder, *Battery materials for ultrafast charging and discharging.* Nature, 2009. **458**(7235): p. 190-193.
4. Lu, L., et al., *A review on the key issues for lithium-ion battery management in electric vehicles.* Journal of power sources, 2013. **226**: p. 272-288.
5. Etacheri, V., et al., *Challenges in the development of advanced Li-ion batteries: a review.* Energy & Environmental Science, 2011. **4**(9): p. 3243-3262.
6. Zhang, S.S., *A review on the separators of liquid electrolyte Li-ion batteries.* Journal of Power Sources, 2007. **164**(1): p. 351-364.
7. Aurbach, D., et al., *A short review of failure mechanisms of lithium metal and lithiated graphite anodes in liquid electrolyte solutions.* Solid state ionics, 2002. **148**(3): p. 405-416.
8. Bruce, P.G., et al., *Li-O2 and Li-S batteries with high energy storage.* Nat Mater, 2012. **11**(1): p. 19-29.
9. Barghamadi, M., A. Kapoor, and C. Wen, *A Review on Li-S Batteries as a High Efficiency Rechargeable Lithium Battery.* Journal of The Electrochemical Society, 2013. **160**(8): p. A1256-A1263.
10. Lin, Z. and C. Liang, *Lithium-sulfur batteries: from liquid to solid cells.* Journal of Materials Chemistry A, 2015. **3**(3): p. 936-958.

11. Bruce, P.G., et al., *Li-O2 and Li-S batteries with high energy storage.* Nature materials, 2012. **11**(1): p. 19-29.
12. Lin, Z. and C. Liang, *Lithium–sulfur batteries: from liquid to solid cells.* Journal of Materials Chemistry A, 2015. **3**(3): p. 936-958.
13. Angulakshmi, N. and A.M. Stephan, *Efficient Electrolytes for Lithium–Sulfur Batteries.* Frontiers in Energy Research, 2015. **3**: p. 17.
14. Kolosnitsyn, V. and E. Karaseva, *Lithium-sulfur batteries: Problems and solutions.* Russian Journal of Electrochemistry, 2008. **44**(5): p. 506-509.
15. Mikhaylik, Y.V. and J.R. Akridge, *Polysulfide Shuttle Study in the Li/S Battery System.* Journal of The Electrochemical Society, 2004. **151**(11): p. A1969-A1976.
16. Zhang, S.S., *Liquid electrolyte lithium/sulfur battery: Fundamental chemistry, problems, and solutions.* Journal of Power Sources, 2013. **231**(0): p. 153-162.
17. Yang, X., et al., *Sulfur-Infiltrated Graphene-Based Layered Porous Carbon Cathodes for High-Performance Lithium–Sulfur Batteries.* ACS Nano, 2014. **8**(5): p. 5208-5215.
18. Xu, J., et al., *Sulfur–Graphene Nanostructured Cathodes via Ball-Milling for High-Performance Lithium–Sulfur Batteries.* ACS Nano, 2014. **8**(10): p. 10920-10930.
19. Ji, X., K.T. Lee, and L.F. Nazar, *A highly ordered nanostructured carbon-sulphur cathode for lithium-sulphur batteries.* Nat Mater, 2009. **8**(6): p. 500-506.
20. Li, X.; Cao, Y.; Qi, W.; Saraf, L. V.; Xiao, J.; Nie, Z.; Mietek, J.; Zhang, J. G.; Schwenzer, B.; Liu, J. J. Mater. Chem. A 2011, 21, 16603.
21. Ji, X., K.T. Lee, and L.F. Nazar, *A highly ordered nanostructured carbon–sulphur cathode for lithium–sulphur batteries.* Nature materials, 2009. **8**(6): p. 500-506.

22. Wang, H.; Yang, Y.; Liang, Y.; Robinson, J. T.; Li, Y.; Jackson, A.; Cui, Y.; Dai, H. Nano Lett. 2011, 11, 2644.

23. Wang, J. Z.; Lu, L.; Choucair, M.; Stride, J. A.; Xu, X.; Liu, H. K. J. Power Sources 2011, 196, 7030.

24. Bin Li, Songmei Li, Jianhua Liu, Bo Wang, and Shubin Yang, Vertically Aligned Sulfur–Graphene Nanowalls on Substrates for Ultrafast Lithium–Sulfur Batteries *Nano Lett.*, 2015, *15* (5), pp 3073–3079

25. Manthiram, A., et al., *Rechargeable Lithium–Sulfur Batteries.* Chemical Reviews, 2014. **114**(23): p. 11751-11787

26. Xiao, L., et al., *A soft approach to encapsulate sulfur: polyaniline nanotubes for lithium-sulfur batteries with long cycle life.* Advanced Materials, 2012. **24**(9): p. 1176-1181.

27. Yuan Yang, Guihua Yu, Judy J. Cha, Hui Wu, Michael Vosgueritchian, Yan Yao†, Zhenan Bao, and Yi Cui, Improving the Performance of Lithium–Sulfur Batteries by Conductive Polymer Coating, *ACS Nano*, 2011, *5* (11), pp 9187–9193

28. Zhang, B., et al., *Enhancement of long stability of sulfur cathode by encapsulating sulfur into micropores of carbon spheres.* Energy & Environmental Science, 2010. **3**(10): p. 1531-1537.

29. Ji, X., K.T. Lee, and L.F. Nazar, *A highly ordered nanostructured carbon-sulphur cathode for lithium-sulphur batteries.* Nat Mater, 2009. **8**(6): p. 500-6.

30. Schuster, J., et al., *Spherical Ordered Mesoporous Carbon Nanoparticles with High Porosity for Lithium–Sulfur Batteries.* Angewandte Chemie International Edition, 2012. **51**(15): p. 3591-3595.

31. Jayaprakash, N., et al., *Porous Hollow Carbon@Sulfur Composites for High-Power Lithium–Sulfur Batteries.* Angewandte Chemie International Edition, 2011. **50**(26): p. 5904-5908.
32. Guo, J., Y. Xu, and C. Wang, *Sulfur-Impregnated Disordered Carbon Nanotubes Cathode for Lithium–Sulfur Batteries.* Nano Letters, 2011. **11**(10): p. 4288-4294.
33. Zheng, G., et al., *Hollow Carbon Nanofiber-Encapsulated Sulfur Cathodes for High Specific Capacity Rechargeable Lithium Batteries.* Nano Letters, 2011. **11**(10): p. 4462-4467.
34. Li, N., et al., *High-rate lithium-sulfur batteries promoted by reduced graphene oxide coating.* Chemical Communications, 2012. **48**(34): p. 4106-4108.
35. Ji, L., et al., *Graphene Oxide as a Sulfur Immobilizer in High Performance Lithium/Sulfur Cells.* Journal of the American Chemical Society, 2011. **133**(46): p. 18522-18525.
36. Elazari, R., et al., *Sulfur-Impregnated Activated Carbon Fiber Cloth as a Binder-Free Cathode for Rechargeable Li-S Batteries.* Advanced Materials, 2011. **23**(47): p. 5641-5644.
37. Barchasz, C., et al., *New insights into the limiting parameters of the Li/S rechargeable cell.* Journal of Power Sources, 2012. **199**(0): p. 322-330.
38. Cheon, S.-E., et al., *Rechargeable Lithium Sulfur Battery: II. Rate Capability and Cycle Characteristics.* Journal of The Electrochemical Society, 2003. **150**(6): p. A800-A805.
39. Li, L., et al., *Enhanced Cycling Stability of Lithium Sulfur Batteries Using Sulfur–Polyaniline–Graphene Nanoribbon Composite Cathodes.* ACS Applied Materials & Interfaces, 2014. **6**(17): p. 15033-15039.

40. Xu, R., et al., *Insight into Sulfur Reactions in Li–S Batteries.* ACS Applied Materials & Interfaces, 2014. **6**(24): p. 21938-21945.

41. Li, W., et al., *V2O5 Polysulfide Anion Barrier for Long-Lived Li–S Batteries.* Chemistry of Materials, 2014. **26**(11): p. 3403-3410.

42. Demir-Cakan, R., et al., *Cathode Composites for Li–S Batteries via the Use of Oxygenated Porous Architectures.* Journal of the American Chemical Society, 2011. **133**(40): p. 16154-16160.

43. Babu, G., et al., *Electrocatalysis of Lithium Polysulfides: Current Collectors as Electrodes in Li/S Battery Configuration.* Scientific reports, 2015. **5**.

44. Deng, Z., et al., *A sulfur–carbon composite for lithium/sulfur battery based on activated vapor-grown carbon fiber.* Solid State Ionics, 2013. **238**(0): p. 44-49.

45. Lv, D., et al., *High performance Li-ion sulfur batteries enabled by intercalation chemistry.* Chemical Communications, 2015. **51**(70): p. 13454-13457.

46. Yang, Y., et al., *New Nanostructured Li2S/Silicon Rechargeable Battery with High Specific Energy.* Nano Letters, 2010. **10**(4): p. 1486-1491.

47. Yan, Y., et al., *High-safety lithium-sulfur battery with prelithiated Si/C anode and ionic liquid electrolyte.* Electrochimica Acta, 2013. **91**(0): p. 58-61.

48. Hassoun, J. and B. Scrosati, *A High-Performance Polymer Tin Sulfur Lithium Ion Battery.* Angewandte Chemie International Edition, 2010. **49**(13): p. 2371-2374.

49. Liu, S., et al., *Lithium-rich Li2.6BMg0.05 alloy as an alternative anode to metallic lithium for rechargeable lithium batteries.* Electrochimica Acta, 2011. **56**(24): p. 8900-8905.

50. Lee, Y.M., et al., *Electrochemical performance of lithium/sulfur batteries with protected Li anodes.* Journal of Power Sources, 2003. **119–121**(0): p. 964-972.

51. Demir-Cakan, R., et al., *Li-S batteries: simple approaches for superior performance.* Energy & Environmental Science, 2013. **6**(1): p. 176-182.
52. Zhang, S.S., *Role of LiNO3 in rechargeable lithium/sulfur battery.* Electrochimica Acta, 2012. **70**: p. 344-348.
53. Aurbach, D., et al., *On the Surface Chemical Aspects of Very High Energy Density, Rechargeable Li–Sulfur Batteries.* Journal of The Electrochemical Society, 2009. **156**(8): p. A694-A702.
54. Lin, Z., et al., *Phosphorous Pentasulfide as a Novel Additive for High-Performance Lithium-Sulfur Batteries.* Advanced Functional Materials, 2013. **23**(8): p. 1064-1069.
55. Zhang, S.S. and J.A. Read, *A new direction for the performance improvement of rechargeable lithium/sulfur batteries.* Journal of Power Sources, 2012. **200**: p. 77-82.
56. Helen, M., et al., *Single step transformation of sulphur to Li2S2/Li2S in Li-S batteries.* Scientific reports, 2015. **5**.
57. Seh, Z.W., et al., *Sulphur–TiO2 yolk–shell nanoarchitecture with internal void space for long-cycle lithium–sulphur batteries.* Nature communications, 2013. **4**: p. 1331.
58. Jayaprakash, N., et al., *Porous Hollow Carbon@ Sulfur Composites for High-Power Lithium–Sulfur Batteries.* Angewandte Chemie, 2011. **123**(26): p. 6026-6030.
59. Yan, Z., et al., *Mesoporous graphene-like nanobowls as Pt electrocatalyst support for highly active and stable methanol oxidation.* Journal of Power Sources, 2015. **284**(0): p. 497-503.
60. Soo, L.T., et al., *An Overview of the Electrochemical Performance of Modified Graphene Used as an Electrocatalyst and as a Catalyst Support in Fuel Cells.* Applied Catalysis A: General, (0).

61. Unni, S.M., V.K. Pillai, and S. Kurungot, *3-Dimensionally self-assembled single crystalline platinum nanostructures on few-layer graphene as an efficient oxygen reduction electrocatalyst.* RSC Advances, 2013. **3**(19): p. 6913-6921.

62. Ballesteros Katemann, B., et al., *Localised electrochemical impedance spectroscopy with high lateral resolution by means of alternating current scanning electrochemical microscopy.* Electrochemistry Communications, 2002. **4**(2): p. 134-138.

63. Macdonald, J.R., *Impedance spectroscopy.* Annals of Biomedical Engineering. **20**(3): p. 289-305.

64. Nadjo, L. and J.M. Savéant, *Linear sweep voltammetry: Kinetic control by charge transfer and/or secondary chemical reactions: I. Formal kinetics.* Journal of Electroanalytical Chemistry and Interfacial Electrochemistry, 1973. **48**(1): p. 113-145.

65. Anderson, A.B. and Y. Cai, *Calculation of the Tafel Plot for H2 Oxidation on Pt(100) from Potential-Dependent Activation Energies.* The Journal of Physical Chemistry B, 2004. **108**(52): p. 19917-19920.

66. Stanjek, H. and W. Häusler, *Basics of X-ray Diffraction.* Hyperfine Interactions. **154**(1): p. 107-119

67. Yamada, K., *Basics of analytical methods used for the investigation of interaction mechanism between cements and superplasticizers.* Cement and Concrete Research, 2011. **41**(7): p. 793-798.

68. Jost, O., et al., *Diameter grouping in bulk samples of single-walled carbon nanotubes from optical absorption spectroscopy.* Applied Physics Letters, 1999. **75**(15): p. 2217-2219

69. Williams, D. and C.B. Carter, *The Transmission Electron Microscope*, in *Transmission Electron Microscopy*. 1996, Springer US. p. 3-17.

70. Saleh, I.M., et al., *Adhesion of Endodontic Sealers: Scanning Electron Microscopy and Energy Dispersive Spectroscopy.* Journal of Endodontics, 2003. **29**(9): p. 595-601.

71. Pantano, C.G. and T.E. Madey, *Electron beam damage in Auger electron spectroscopy.* Applications of Surface Science, 1981. **7**(1): p. 115-141

72. Hollander, J.M. and W.L. Jolly, *X-ray photoelectron spectroscopy.* Accounts of Chemical Research, 1970. **3**(6): p. 193-200.

73. Schneider, H., et al., *Influence of different electrode compositions and binder materials on the performance of lithium–sulfur batteries.* Journal of Power Sources, 2012. **205**(0): p. 420-425.

74. Mikhaylik, Y.V. and J.R. Akridge, *Polysulfide Shuttle Study in the Li/S Battery System.* Journal of The Electrochemical Society, 2004. **151**(11): p. A1969-A1976.

75. Wu, F., et al., *Sulfur/Polythiophene with a Core/Shell Structure: Synthesis and Electrochemical Properties of the Cathode for Rechargeable Lithium Batteries.* The Journal of Physical Chemistry C, 2011. **115**(13): p. 6057-6063.

76. Li, G.-C., et al., *A Polyaniline-Coated Sulfur/Carbon Composite with an Enhanced High-Rate Capability as a Cathode Material for Lithium/Sulfur Batteries.* Advanced Energy Materials, 2012. **2**(10): p. 1238-1245.

77. Ma, G., et al., *A lithium anode protection guided highly-stable lithium-sulfur battery.* Chemical Communications, 2014. **50**(91): p. 14209-14212.

78. Bhatt, M.D., et al., *Key scientific challenges in current rechargeable non-aqueous Li–O 2 batteries: experiment and theory.* Physical Chemistry Chemical Physics, 2014. **16**(24): p. 12093-12130.

79. Fang, R., et al., *Localized polyselenides in a graphene-coated polymer separator for high rate and ultralong life lithium-selenium batteries.* Chemical Communications, 2015. **51**(17): p. 3667-3670.

80. Bonaccorso, F., et al., *Graphene, related two-dimensional crystals, and hybrid systems for energy conversion and storage.* Science, 2015. **347**(6217).

81. Li, Z., et al., *A Highly Ordered Meso@Microporous Carbon-Supported Sulfur@Smaller Sulfur Core–Shell Structured Cathode for Li–S Batteries.* ACS Nano, 2014. **8**(9): p. 9295-9303.

82. He, G., et al., *Tailoring Porosity in Carbon Nanospheres for Lithium–Sulfur Battery Cathodes.* ACS Nano, 2013. **7**(12): p. 10920-10930.

83. Liang, C., N.J. Dudney, and J.Y. Howe, *Hierarchically Structured Sulfur/Carbon Nanocomposite Material for High-Energy Lithium Battery.* Chemistry of Materials, 2009. **21**(19): p. 4724-4730.

84. Dorfler, S., et al., *High capacity vertical aligned carbon nanotube/sulfur composite cathodes for lithium-sulfur batteries.* Chemical Communications, 2012. **48**(34): p. 4097-4099.

85. Yang, Y., et al., *Improving the performance of lithium–sulfur batteries by conductive polymer coating.* Acs Nano, 2011. **5**(11): p. 9187-9193.

86. Pang, Q., et al., *Surface-enhanced redox chemistry of polysulphides on a metallic and polar host for lithium-sulphur batteries.* Nat Commun, 2014. **5**.

87. Liang, X., et al., *A highly efficient polysulfide mediator for lithium–sulfur batteries.* Nat Commun, 2015. **6**.

88. Liang, Z., et al., *Sulfur Cathodes with Hydrogen Reduced Titanium Dioxide Inverse Opal Structure.* ACS Nano, 2014. **8**(5): p. 5249-5256.

89. Guo, S., S. Dong, and E. Wang, *Three-Dimensional Pt-on-Pd Bimetallic Nanodendrites Supported on Graphene Nanosheet: Facile Synthesis and Used as an Advanced Nanoelectrocatalyst for Methanol Oxidation.* ACS Nano, 2010. **4**(1): p. 547-555.

90. Bhaviripudi, S., et al., *Role of Kinetic Factors in Chemical Vapor Deposition Synthesis of Uniform Large Area Graphene Using Copper Catalyst.* Nano Letters, 2010. **10**(10): p. 4128-4133.

91. Chi Linh, D., et al., *Properties of Pt/C nanoparticle catalysts synthesized by electroless deposition for proton exchange membrane fuel cell.* Advances in Natural Sciences: Nanoscience and Nanotechnology, 2013. **4**(3): p. 035011.

92. Song, J., et al., *Strong Lithium Polysulfide Chemisorption on Electroactive Sites of Nitrogen-Doped Carbon Composites For High-Performance Lithium–Sulfur Battery Cathodes.* Angewandte Chemie International Edition, 2015. **54**(14): p. 4325-4329.

93. Diao, Y., et al., *Insights into Li-S Battery Cathode Capacity Fading Mechanisms: Irreversible Oxidation of Active Mass during Cycling.* Journal of The Electrochemical Society, 2012. **159**(11): p. A1816-A1821.

94. Tung-Yuan, Y., L. Jer-Yeu, and L. Ling-Kang, *Nanocomposite for methanol oxidation: synthesis and characterization of cubic Pt nanoparticles on graphene sheets.* Science and Technology of Advanced Materials, 2013. **14**(3): p. 035001.

95. Chen, W.-F., J.T. Muckerman, and E. Fujita, *Recent developments in transition metal carbides and nitrides as hydrogen evolution electrocatalysts.* Chemical Communications, 2013. **49**(79): p. 8896-8909.

96. Kitchin, J.R., et al., *Trends in the chemical properties of early transition metal carbide surfaces: A density functional study.* Catalysis Today, 2005. **105**(1): p. 66-73.
97. Nørskov, J.K., et al., *Density functional theory in surface chemistry and catalysis.* Proceedings of the National Academy of Sciences, 2011. **108**(3): p. 937-943.
98. Chen, J.G., *Carbide and Nitride Overlayers on Early Transition Metal Surfaces: Preparation, Characterization, and Reactivities.* Chemical Reviews, 1996. **96**(4): p. 1477-1498.
99. Pozio, A., et al., Comparison of high surface Pt/C catalysts by cyclic voltammetry. Journal of power sources, 2002. 105(1): p. 13-19.
100. Voiry, D., et al., Enhanced catalytic activity in strained chemically exfoliated WS2 nanosheets for hydrogen evolution. Nat Mater, 2013. 12(9): p. 850-855.
101. Berkdemir, A., et al., Identification of individual and few layers of WS2 using Raman Spectroscopy. Scientific Reports, 2013. 3: p. 1755.

ABSTRACT

ELECTROCATALYSIS IN LI-S BATTERIES

by

HESHAM I. A. AL SALEM

May 2016

Advisor: Dr. Leela Mohana Reddy Arava

Major: Mechanical Engineering

Degree: Doctor of Philosophy

Stabilizing polysulfide-shuttle process while ensuring high sulfur loading holds the key to realize high theoretical energy density (2500 Wh/kg) of lithium-sulfur (Li-S) batteries. Though several carbon based porous materials have been used as host structures for sulfur and its intermediate polysulfides, the week adsorption of polysulfides on carbon surface and its poor reaction kinetics limits them from practical application. Here, we preset a novel electcatalysis approach to stabilize polysulfide shuttle process and also enhance its red-ox kinetics. As a proof of concept, we have studied in-detail using conventional electrocatalyst (Pt/graphene composite), further the same extended to cost-effective electrocatalysts such as WS_2 nanosheets and Metal carbides for viable practical applications. Nature of electrocatalyst, concentration of polysulfides and temperature of the cell on electrochemical properties will be discussed. We reveal substantial improvement in electrochemical properties such as specific capacity, rate capability, and coulombic efficiency and corroborate our findings with systematic experimental studies. Interaction between electrocatalyst and polysulfides has been evaluated by conducting X-ray photoelectron spectroscopy and electron microscopy studies at various electrochemical conditions.

As a conclusion, introducing a catalyst in the Li−S system will open a new avenue for improving electrochemical performance.

AUTOBIOGRAPHICAL STATEMENT

Dr. Al Salem was born in Irbid, Jordan on January, 5 1973. He received his Bachelor and Master degree in mechanical engineering from Jordan University of Science and Technology, Jordan in 1996 and 1999; respectively.